

Emerging van der Waals ferroelectrics: Unique properties and novel devices

Cite as: Appl. Phys. Rev. **8**, 021316 (2021); <https://doi.org/10.1063/5.0028079>

Submitted: 02 September 2020 • Accepted: 24 March 2021 • Published Online: 27 May 2021

 Fei Xue, Jr-Hau He and  Xixiang Zhang

COLLECTIONS

 This paper was selected as Featured



[View Online](#)



[Export Citation](#)



[CrossMark](#)

ARTICLES YOU MAY BE INTERESTED IN

Strain-tuning of the electronic, optical, and vibrational properties of two-dimensional crystals
Applied Physics Reviews **8**, 021318 (2021); <https://doi.org/10.1063/5.0037852>

Memory applications from 2D materials

Applied Physics Reviews **8**, 021306 (2021); <https://doi.org/10.1063/5.0038013>

Next generation ferroelectric materials for semiconductor process integration and their applications

Journal of Applied Physics **129**, 100901 (2021); <https://doi.org/10.1063/5.0037617>



Applied Physics
Reviews

Read. Cite. Publish. Repeat.

19.162

2020 IMPACT FACTOR*

Emerging van der Waals ferroelectrics: Unique properties and novel devices

Cite as: Appl. Phys. Rev. **8**, 021316 (2021); doi: [10.1063/5.0028079](https://doi.org/10.1063/5.0028079)

Submitted: 2 September 2020 · Accepted: 24 March 2021 ·

Published Online: 27 May 2021



[View Online](#)



[Export Citation](#)



[CrossMark](#)

Fei Xue,^{1,a)}  Jr-Hau He,^{2,a)} and Xiang Zhang^{1,a)} 

AFFILIATIONS

¹Physical Science and Engineering Division, King Abdullah University of Science and Technology, Thuwal 23955-6900, Saudi Arabia

²Department of Materials Science and Engineering, City University of Hong Kong, 26 Kowloon, Hong Kong, China

^{a)}Authors to whom correspondence should be addressed: fei.xue@kaust.edu.sa; jrhauhe@cityu.edu.hk; and xiang.zhang@kaust.edu.sa

ABSTRACT

The past few decades have witnessed extensive and intensive studies on ferroelectric materials with switchable electric polarization due to their broad device applications. Emerging van der Waals (vdW) layered ferroelectrics ingeniously assemble *strong* covalent-bonded polar or non-polar monolayers through *weak* vdW forces. These atom arrangements contrast with the stacking of conventional oxide ferroelectrics, enabling unprecedented ferroelectric physics in terms of polarization origin, polar stabilization, and switching kinetics. Combined with other inherent optical and electrical features, the vdW ferroelectrics can undoubtedly provide a new, versatile platform for advancing fundamental physics and revolutionizing device technology. In this review, we summarize the unique ferroelectric properties in experimentally confirmed vdW ferroelectrics, particularly those properties that expand our understanding of ferroelectric switching. We also elucidate how some of these properties can intrinsically reduce depolarized instability at the atomic limit. Finally, we discuss innovative devices enabled by distinct properties of vdW ferroelectrics for electronic, optoelectronic, and energy-harvesting applications, and highlight possible future research lines.

© 2021 Author(s). All article content, except where otherwise noted, is licensed under a Creative Commons Attribution (CC BY) license (<http://creativecommons.org/licenses/by/4.0/>). <https://doi.org/10.1063/5.0028079>

TABLE OF CONTENTS

I. INTRODUCTION	1
II. UNIQUE FERROELECTRIC PROPERTIES	3
A. Interlayer-charge-transfer-induced polarization ..	3
B. Dipole locking stabilized polarization	5
C. Quadruple-well potential	6
1. Giant negative piezoelectricity	8
2. Inverse polarization switching	9
D. Piezoelectric domain walls	9
E. Gate-tunable polarization.....	10
III. NOVEL FERROELECTRIC DEVICES	11
A. Multidirectional switchable memristors	12
B. Optoelectronic ferroelectric memories	12
C. Ferroelectric semiconductor transistors.....	13
D. VdW ferroelectric heterostructure-based devices ..	14
E. Piezoelectric nanogenerators with flexible design ..	15
IV. SUMMARY AND OUTLOOK	16

I. INTRODUCTION

Ferroelectrics are a class of materials that feature spontaneous electric polarization (i.e., dipole or polar ordering), which can be reversibly

switched by applying an external electric field,¹ mechanical strain,² or light irradiation.³ Although the first ferroelectric (i.e., Rochelle salt crystal) was reported in 1920, the boom in the development of ferroelectrics for theoretical modeling, creative synthesis, and disruptive applications did not commence until the discovery of barium titanate ferroelectric crystals during World War II.⁴ In the following years, preliminary phenomenological models were established to describe ferroelectric switching and, by using bulk ferroelectrics, device applications were initially demonstrated. By the late 1980s, the realization of high-quality thin-film ferroelectrics and the maturity in their processing greatly prompted device use. Since the 1990s, with the discovery of many new ferroelectrics and significant improvements in the material's quality, a plethora of ferroelectric applications have been successfully demonstrated, including memories, radio frequency devices, low-power field-effect transistors, solar cells, and actuators.⁵ Some of these applications have already been commercialized for practical use. For example, a ferroelectric PbTiO₃ film sandwiched between two electrodes can be densely integrated into 8 Mbit ferroelectric chips for information storage. These significant achievements in device applications necessitate an in-depth understanding of their building blocks (i.e., ferroelectrics) to spur pivotal fundamental advances, such as the atomic investigation of the polarization origin.

Over recent decades, fundamental studies in the ferroelectric realm have suggested that the material backbone is the family of ABO_3 structured oxides (oxide ferroelectrics), such as BaFeO_3 and PbTiO_3 .^{6–11} Transmission electron microscope images^{12–14} have shown their spontaneous polarization arises phenomenologically from the off-centered B ions, i.e., structural distortion. This intrinsic polarization involves the collective interaction of short-range electron-repulsive forces which favors the formation of paraelectric ordering, and long-range Coulomb coupling which stabilizes the ferroelectric ordering.^{15,16} Their dynamic interaction can be described by the well-known Landau–Ginzburg–Devonshire model, i.e., double-well potential with respect to the polarization, which illustrates a distorted crystal structure over a symmetric structure.^{17,18} In this model, there are two minima which are widely considered to be two stable polarization states, and to switch between them, an energy barrier must be overcome.

In reality, the ferroelectric polarization, P , electrostatically induces bound charges $\rho = \text{div } P$ at film interfaces, which can, in turn, create an inner electric field across the ferroelectric body, i.e., the depolarization field. Its direction is, however, opposite to that of ferroelectric polarization, which inevitably adds instability (apart from the mesoscopic electron-repulsive force) to the structural distortion. To maintain the polarization, compensation charges, including those of absorbed interface molecules and free carriers, are necessarily required to screen the depolarization field. Supposing that the bound charges related to this field are not completely neutralized, the intrinsic polarization can consequently be destabilized.^{17,19} In particular, while the thickness of ferroelectric films is reduced to several nanometers below the critical thickness, the magnitude of the depolarization field significantly increases, and its influence on ferroelectric instability dramatically intensifies, given that the polarization charges remain nearly constant with variation in thickness. As a result, for most ferroelectrics, 2D polarization may entirely vanish. Thus, the depolarization field poses a huge challenge to the existence of ultrathin ferroelectrics, particularly unit cell-thick oxide ferroelectrics. To effectively combat this notorious field and achieve atomic-scale polarization, a range of viable approaches has been successively proposed.^{1,20–22} For instance, an epitaxial strain induced by the substrate can markedly enhance polarization and oppose depolarized instability at a nanoscale thickness, whereas the rationally introduced compensation charges from conductive electrodes can largely screen bound charges. Nevertheless, all of these approaches involve the integration of external elements with ferroelectrics, limiting the stabilization of free-standing ultrathin ferroelectrics.

The exploration of new ferroelectric systems beyond oxide counterparts, such as van der Waals (vdW) ferroelectrics, has the potential to enrich the understanding of ferroelectric physics and stabilize polarization around the atomic limit through the material's inherent physics. In 1994, the first vdW-layered ferroelectric, i.e., CuInP_2S_6 , was discovered in a bulk form with a millimeter thickness,²³ far from the thinness required for probing quantum ferroelectrics. In the following two decades, research on vdW ferroelectrics with a reduced dimensionality, however, remained stagnant. Since 2015, fueled by 2D material studies, the vdW CuInP_2S_6 crystal with ionic conductivity has gradually attracted increasing attention^{24,25} and demonstrated stable polarization down to 4 nanometers. Nearly simultaneously, theoretical works predicted the existence of 2D free-standing vdW ferroelectrics,

including monolayer $\alpha\text{-In}_2\text{Se}_3$ and monolayer SnS.^{26–30} Shortly thereafter, their experimental breakthroughs have been made with the findings that the unique dipoles can help conquer the depolarization field.^{31–35} Strikingly, in 2018, 2D ferroelectric polarization and metallicity, which for a long time were believed to be a paradox, were unambiguously demonstrated to exist in 1T WTe_2 as thin as a bilayer,³⁶ indicating new strategies for preserving 2D polarization. Over the past few years, in addition to the results of novel quantum ferroelectric physics, the accomplishments of vdW ferroelectrics have encompassed the architectural innovation and performance optimization of conventional memory, logic, and energy-harvesting devices. These pioneering early studies^{27,30,37–55} have suggested that the emerging vdW ferroelectrics, albeit still in their infancy, are an unparalleled platform for the quest of 2D quantum physics and disruptive technology.

Within a vdW ferroelectric, weak vdW forces bind each monolayer together across vdW gaps while strong intralayer covalent bonds govern the monolayers. These delicate crystal assemblies (Fig. 1 shows a comparison with oxide ferroelectrics) allow the polarization switching in vdW ferroelectrics to exhibit impressive hallmarks, which are typically absent in oxide ferroelectrics. More importantly, particularly for sustaining ultimate thin polarization (Fig. 1), some of these hallmarks demonstrate promising approaches to contend with the depolarization field; some of these resulting features also expand our understanding of polarization origin, polarization stabilization, and switching kinetics owing to the weak interlayer interaction and the periodic vdW gaps. In addition, the newly discovered vdW ferroelectric properties are significantly enriched by the material's other native physical or chemical phenomena. For example, the fine incorporation of polarized antiferroelectric domains into ferroelectric domains gives rise to unusual piezoelectric domain walls.⁵⁶ The natural combination of semiconducting (or conducting) and ferroelectric behaviors enables ferroelectricity to be manipulatable in a transistor architecture through leveraging a gate bias.^{36,41,43,57}

Moreover, the vdW ferroelectrics also possess prominent merits that may encourage device innovation in the post-Moore era. The nanodevices based on vdW ferroelectric can be freely fabricated on various substrates including silicon, polymers, and ceramics, but they retain excellent downscaling due to the nature of their material geometry. By contrast, most oxide-ferroelectric-based devices reside on specific, exclusive epitaxial substrates,^{1,8,9,14} such as SrTiO_3 , which greatly limits their practical applications. Meanwhile, with the thickness downscaling, the vdW ferroelectrics exhibit largely tunable bandgaps while covering the solar spectrum,⁵⁸ and are thus anticipated to revitalize the development of high-performance ferroelectric photovoltaic devices.⁵⁹ Furthermore, the cleaved surfaces of vdW ferroelectrics feature no dangling bonds, and therefore, they allow for the construction of ideal interfaces with two or more assembled dissimilar materials in heterostructure device applications.

The study of vdW ferroelectrics is currently on the rise. Previous research has preliminarily demonstrated their unusual ferroelectric physics and advanced device applications. It is urgent to highlight these great achievements and draw more attention to this burgeoning field. A systematic review on this topic, however, has not yet appeared. Here, we mainly focus on the progress that has been made in experimentally confirmed vdW ferroelectrics. We interpret their unique ferroelectric physics in detail and describe why their atomic-limit polarization can survive in contrast to oxide ferroelectrics. We also

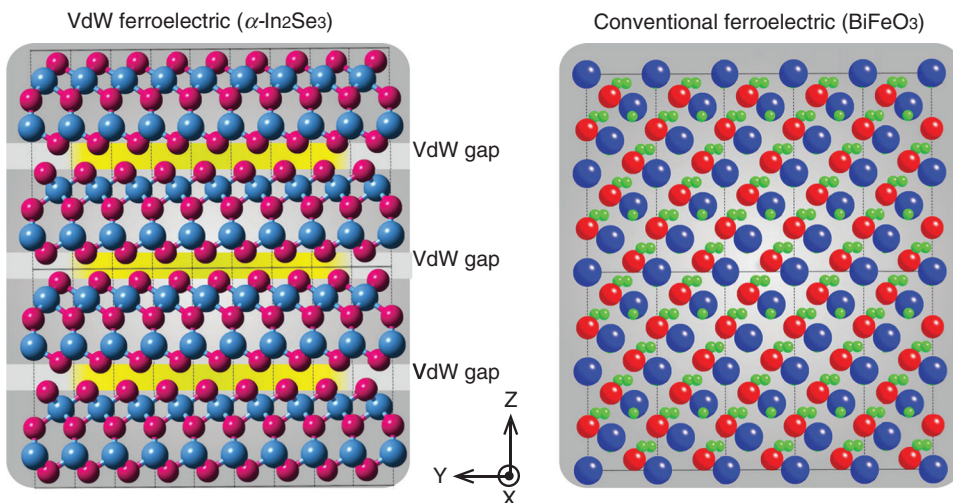


FIG. 1. Schematic comparison of crystal structures of a typical vdW ferroelectric (i.e., hexagonal α -In₂Se₃) and a representative conventional ferroelectric (i.e., BiFeO₃). Both structures are presented along the [100] direction. The distinct vdW gaps, for example in α -In₂Se₃, are marked by yellow, enabling some unique ferroelectric physics in contrast with conventional ferroelectrics. These vdW gaps also facilitate the mechanical exfoliation from parent crystals for novel heterostructure-device construction.

discuss their distinct prototype devices and give possible future perspectives. We note that thorough reviews of predicted vdW ferroelectrics can be found in other literature.^{60–63}

II. UNIQUE FERROELECTRIC PROPERTIES

The unique vdW ferroelectric switching that has been reported can be briefly summarized into the following five aspects. First, a new origin of switchable polarization, i.e., the interlayer-charge-transfer effect, has been found in a polar metal 1T' WTe₂. Second, a novel stabilization mechanism of switchable polarization, i.e., the dipole locking effect, has been demonstrated in α -In₂Se₃. Third, a new kinetics of switchable polar ordering, i.e., the quadruple-well potential effect, has been unveiled in CuInP₂S₆, which accompanies the emergence of negative piezoelectricity and inverse ferroelectric switching. Fourth, a new piezoelectric domain wall has been found in CuInP₂S₆. Fifth, a strategy for polarization manipulation, i.e., gate tunability, has been reported in several vdW ferroelectrics.

A. Interlayer-charge-transfer-induced polarization

In this section, we examine the interlayer-charge-transfer in vdW 1T' WTe₂, which is an entirely different polarization origin. 1T' WTe₂ holds a distorted common hexagonal structure, whereas its multilayer crystal structure is non-centrosymmetric [Fig. 2(a)]. Although the non-centrosymmetry is normally needed for ferroelectric distortion, 1T' WTe₂'s polarization switching kinetics under an applied electric field is indeed involved with vertical charge transfer across each layer, instead of structural distortion.^{36,64,65} We again stress that, for oxide ferroelectrics, structural distortion is the common origin of spontaneous electric polarization. Thus, the interlayer-charge-transfer should be a non-trivial mechanism and presents a new dimension to the field of ferroelectrics.

Fei *et al.* reported that polar semimetal 1T' WTe₂ is an intrinsic ferroelectric with out-of-plane (OOP) polarization.³⁶ This groundbreaking discovery indicates that ferroelectricity and metallicity are subtly incorporated into a 2D material, overturning a long-held belief that these two exclusive features could not mutually coexist because of the electron screening of long-range Coulomb forces.⁶⁶ In 1T' WTe₂,

the switchable polarization can survive down to the bilayer thickness, which is phenomenally attributed to the following reasons. First, the 1T' WTe₂ crystal possesses vdW stacking and a unique atom stacking which therefore provides the structural prerequisite for interlayer-charge-transfer effect. Second, this completely new regime of polarization switching does not intertwine with the destabilization from mutual interactions among the long-range Coulomb force, the depolarization field, and the large number of mobile electrons. We stress that, for oxide ferroelectrics, these three factors strongly affect the formation of 2D polarization; albeit favorable for the screening to the depolarization field at interfaces, the mobile electrons particularly from material interior have a detrimental effect on long-range Coulomb forces.⁶⁷ Third, the free electrons from 1T' WTe₂ itself, as opposed to those from adjacent electrodes in oxide ferroelectrics, enable an effective screening at the bilayer thickness to the depolarization field but probably not to the interlayer-charge-transfers. We note that the old belief that ferroelectric metal does not exist was based on the structurally distorted polar materials. In this respect, the polar metal is a highly correlated system and its polarization closely tied to at least four sets of balances: the competition between the short-range repulsive forces and the long-range Coulomb forces, the competition between the interior free carriers (here, we ignore the contribution from the exterior free electrons on electrodes) and the depolarization fields, the competition between the interior free carriers and the long-range Coulomb forces, and the competition between the depolarization field and the long-range Coulomb forces. Consequently, it is plausible that the polarization in a metal would vanish. Fortunately, the 1T' WTe₂ is, though, a ferroelectric semimetal but with a different polarization origin. Most of these complex interactions do not associate with its polarization, largely reducing destabilization and facilely achieving 2D polarization.

Yang *et al.* theoretically unraveled the interlayer charge transfer effect in 1T' WTe₂.⁶⁵ As revealed in Fig. 2(a), two stable polarization states (i.e., state I and state II) can be reversed to each other via the structural mirror operation along the horizontal plane. A slight interlayer translation is predicted as a first step to achieve the most effective pathway. For the state I crystal structure, the horizontal distance

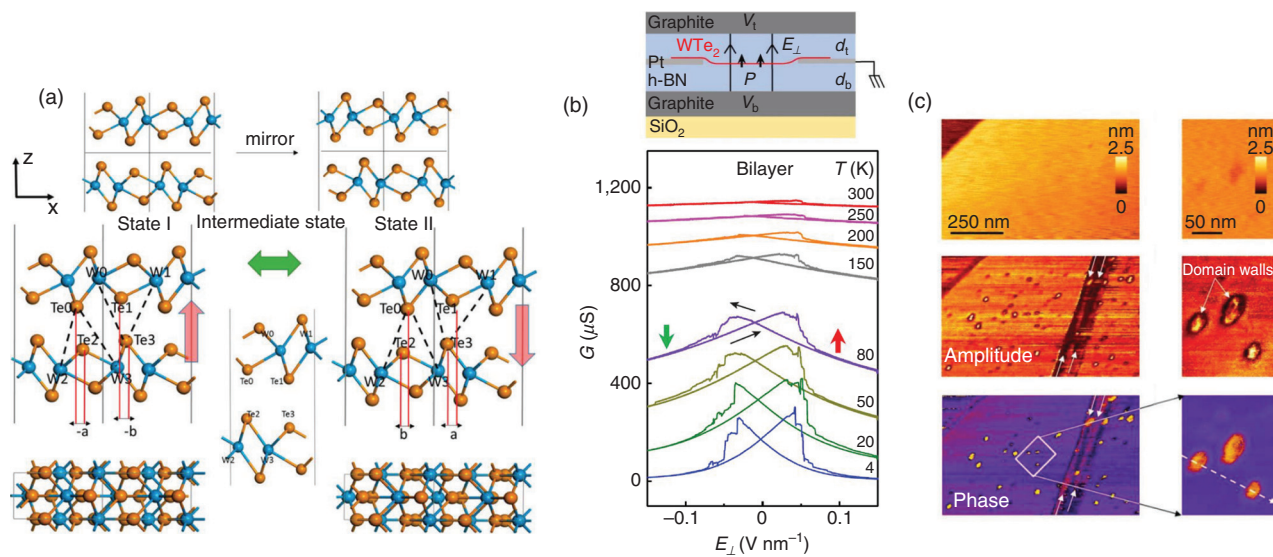


FIG. 2. Charge transfer effect in vdW WTe₂ (a) Schematic crystal structures showing two different polarization states of WTe₂. Reproduced with permission from Yang *et al.*, J. Phys. Chem. Lett. **9**, 24 (2018). Copyright 2018 American Chemical Society.⁶⁵ (b) Top: Device geometric structure used in the measurement. Bottom: Conductance G (ferroelectric switching) of a bilayer WTe₂ device as a function of E_{perp}. Reproduced with permission from Fei *et al.*, Nature **560**, 336 (2018). Copyright 2018 Springer Nature.³⁶ (c) PFM mapping collected from a bulk WTe₂ crystal. The right panel shows the magnified domain images, as indicated by the white rectangle. Reproduced with permission from Sharma *et al.*, Sci. Adv. **5**, eaax5080 (2019). Copyright 2019 American Association for the Advancement of Science.⁶⁸

between Te0 and Te2 is 0.32 Å, whereas that between Te1 and Te3 is slightly more, at 0.4 Å. Moving the upper layer along the +x axis a distance of $0.32 + 0.4 = 0.72$ Å can produce state II. Conversely, as for state II, the distance between Te0 and Te2 is 0.4 Å, whereas that between Te1 and Te3 is 0.32 Å. Slightly shifting the upper layer of state II by 0.72 Å along the -x-axis can give rise to state I. Meanwhile, as a result of the non-centrosymmetric structure in multilayer 1T' WTe₂, the charges on the sites of Te0 and Te3 (or Te1 and Te2) are not strictly equal and will inevitably transfer between these sites during the interconversion of state I and state II. Consequently, the ferroelectric polarization of 1T' WTe₂ is switchable in the OOP direction.

We now proceed to review the experimental demonstrations of OOP ferroelectric polarization in 1T' WTe₂. Fei *et al.* manifested the ferroelectric switching by electrical hysteresis in a sandwiched device geometry that can offer a uniform OOP poling field.³⁶ As shown in Fig. 2(b), when E_{perp} is swept back and forth, electrical curves of a bilayer 1T' WTe₂ device feature hysteresis (i.e., bistability), even at room temperature. However, this remarkable hysteresis can vanish in a monolayer-crystal-based device, consistent with the centrosymmetric nature of monolayer structure. The authors also pointed out that these two comparative experiments firmly rule out the possibility of charge injection into the encapsulated boron nitride (BN) layer. Combined with the charge-density-variation test and theoretical prediction,^{36,65} the polarization switching in 1T' WTe₂ should be closely linked with charge transfer. Note that this electrical hysteresis measurement only verifies that few-layer (e.g., bilayer and trilayer) samples have ferroelectric switching, but nor was switching seen in thicker (e.g., 8 nm) one. The authors ascribe this behavior to the screening of E_{perp} on the nanometer scale within the 1T' WTe₂ metal, i.e., electrostatic screening effect for bulk metal. Based on the aforementioned pioneering work,³⁶ Sharma *et al.* systematically studied bulk 1T' WTe₂ at room

temperature using high-resolution piezoresponse force microscopy (PFM) in an N₂ environment to avoid surface oxidation.⁶⁸ As shown in Fig. 2(c), a thick 1T' WTe₂ crystal exhibits remarkable ferroelectric domains with lines and oval shapes. Note that while visualizing these domains, the variation in height was excluded by the authors based on the smooth surface of 1T' WTe₂. Upon applying an electric field, the 1T' WTe₂ ferroelectric switching loops were unexpectedly observed, overcoming the large leakage current.⁶⁸ Therefore, these unambiguous results confirm that bulk 1T' WTe₂ semimetal should retain room-temperature ferroelectric switching.

The 1T' WTe₂ embraces not only ferroelectric polarization but also other physical properties, such as type II Weyl semimetallicity, 2D spin-torque, and superconductivity.^{69–72} If ferroelectricity and these features are taken into account together, the strong intrinsic correlation may create many new intriguing realms for exploration, for example, the ferroelectric nonlinear anomalous Hall effect. Additionally, 1T' WTe₂'s primary polarization mechanism, namely the interlayer-charger-transfer effect, is predicted to be a ubiquitous phenomenon,⁶⁵ which can also be applied to other paraelectric 2D materials such as graphene⁷³ and hexagonal BN for producing switchable polar ordering by sliding or twisting a single sheet. This prediction is expected to largely broaden the scope for ferroelectric materials beyond the strict restriction to a few non-centrosymmetric ones. To demonstrate this universe origin, further experiments are needed. Another interesting fact is that, among the family of WTe₂, other monolayer semimetals, including 1T' MoTe₂ and 1T' MoS₂, are calculated to retain ferroelectric polarization as well but with the origin of structural distortion,^{28,74} like oxide ferroelectrics. Such a discrepancy results from their different crystal structures transformed from the unstable 1T phase: the 1T' WTe₂ is orthorhombic (space group: Pmn2₁),⁷⁵ the 1T' MoTe₂ is monoclinic (space group: P2₁/m),⁷⁶ and 1T' MoS₂ belongs to

rhombohedral (space group: $P\bar{3}m1$) structure.^{28,77} This structural difference can also be inferred from the fact that the polarization in monolayer WTe₂ vanishes while that in monolayer MoTe₂ surprisingly exists. Although monolayer 1T' MoTe₂ ferroelectric has been explored,⁷⁴ other atomic thin semimetals in the transition-metal dichalcogenides family, such as MoS₂, MoSe₂, and WSe₂, remain to be examined. We note that the report on monolayer OOP polarization in 1T' MoTe₂ reveals that free electrons within the material itself can serve as an interior carrier source to screen the strong depolarization field at a low dimension, indicating an intrinsic approach to stabilize ferroelectricity. This stabilization regime is phenomenologically rational but requires additional experiments to be verified. Furthermore, even though pilot demonstrations have phenomenally suggested that the ferroelectric switching in 1T' WTe₂ arises from interlayer charge transfer, its switching kinetics still lacks in-depth understanding. For example, it is unclear how a vertical poling electrical field can induce an initial lateral displacement within a bilayer WTe₂. Although several theoretical works on the interlayer charge transfer have been published,^{64,65} they all straightforwardly supposed that a lateral interlayer translation exists and did not mention its underlying process. It is also unclear how the free carriers within a semimetal interact with interlayer-transferred charges. The theoretical calculations all assumed that the transferred charges would not be fully neutralized by free carriers. Attention in these directions must be given to dig deeper into the switching mechanism.

B. Dipole locking stabilized polarization

In Sec. II B, we discuss the exotic dipole-stabilization mechanism, termed the dipole locking effect in III-VI compounds in the form of III₂-VI₃ proposed by Xiao *et al.*³² This effect dictates the simultaneous flipping of in-plane (IP) and OOP polarization with an applied electric field that intrinsically stems from the unique covalent bond

configuration. The specific chemical bonds in ferroelectric crystals add a new degree of freedom for stabilizing 2D ferroelectricity and combatting the depolarization field. Hence, monolayer vdW ferroelectrics can unexpectedly sustain polarization at room temperature, despite their polarization restricted in part by the depolarized instability. More importantly, no external elements, including epitaxial strain as in oxide ferroelectrics, are introduced into the monolayer for holding polar ordering. We note that the III-VI ferroelectric compounds still possess the structural distortion origin. Among these compounds, ferroelectric α -In₂Se₃ has received considerable attention^{31–34,37,42,44,45,55,57,60,78–87} and is taken as an example to interpret the effect. The ferroelectric α -In₂Se₃ indeed possesses two polymorphs: a hexagonal structure (2H) and a rhombohedral structure (3R).⁸¹ Both of them preserve IP and OOP polarization at room temperature and exhibit the dipole locking effect.^{32,35,78,80}

It is indispensable to determine the polarization origin of α -In₂Se₃ with crystal non-centrosymmetric analyses. As shown in the left panels of Figs. 3(b) and 3(c), both 2H and 3R α -In₂Se₃ crystals are constituted by the regular stacking of a quintuple layer that is composed of five atom layers in the sequence of Se-In-Se-In-Se. Their structural differences relate to the disparate arrangements between two neighboring quintuple layers: for the 2H structure, the upper quintuple layer can be arranged by first mirroring and then shifting the lower one; for the 3R structure, the upper one can be achieved by solely shifting the lower one without mirroring the operation. Despite the stacking difference, their non-centrosymmetry stems from the different spacing between the central Se atom layer and its two adjacent In atom layers. This unique intralayer covalent bond configuration results in the emergence of their IP and OOP dipoles. Because these two types of perpendicular dipoles share an origin (displacement of an Se atom relative to its neighboring In atoms), the electrical switching of each dipole can render the reversal of the other one, which in principle is termed the “dipole locking effect.” It should be re-emphasized that by

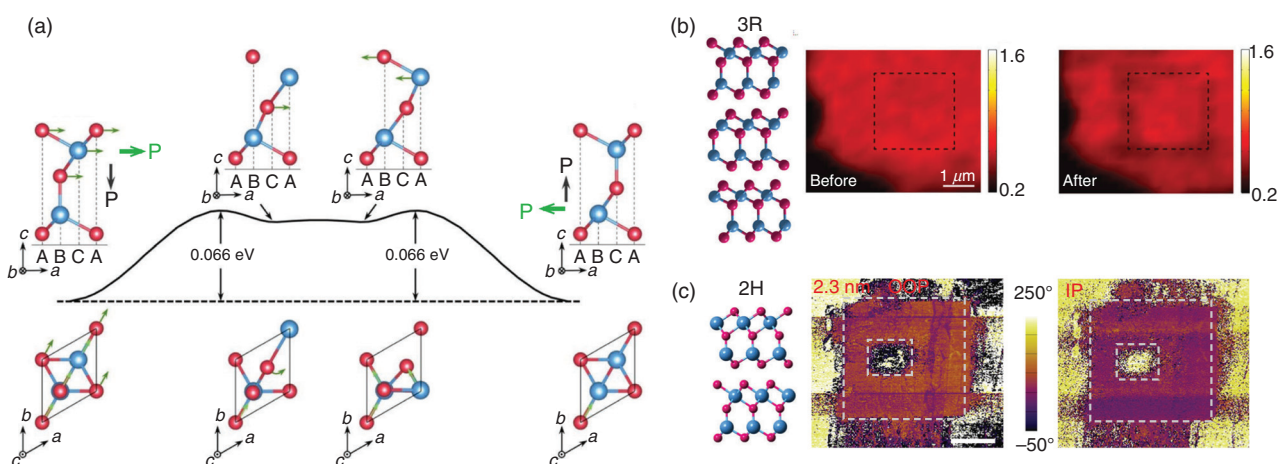


FIG. 3. Dipole locking effect in vdW α -In₂Se₃. (a) Energy profile of the kinetic pathway to interpret simultaneous reversal of the IP and OOP polarization in monolayer α -In₂Se₃. The green and black arrows indicate IP and OOP dipoles, respectively. Reproduced with permission from Ding *et al.*, Nat. Commun. **8**, 14956 (2017). Copyright 2018 Springer Nature.²⁶ (b) SHG mapping before and after a square pattern was written into a dashed area to demonstrate the dipole locking effect in a 3R α -In₂Se₃ sample. Reproduced with permission from Xiao *et al.*, Phys. Rev. Lett. **120**, 227601 (2018). Copyright 2018 American Physical Society.³² (c) IP and OOP PFM phase images after electrically writing two square patterns along the OOP direction to demonstrate the dipole locking effect in 2H α -In₂Se₃ crystal. The sample is 2.3 nm thick. Reproduced with permission from Xue *et al.*, Adv. Funct. Mater. **28**, 1803738 (2018). Copyright 2018 WILEY-VCH.³⁵

this entangling interaction within the quintuple layer, the intralayer dipoles can be delicately stabilized at room temperature. In the case of a multilayered specimen, the vdW gaps may warrant that such intra-layer stabilization receives a small degree of perturbation from inter-layer interactions, and thus, the interlayer influence could be ignored. Generally, the intralayer dipoles can, in part, be deemed as an isolated system, whose stabilization is nearly immune to the neighboring layers in an equilibrium state. Whether the stable, switchable polarization in $\alpha\text{-In}_2\text{Se}_3$ exists does not therefore rigorously depend on sample thickness. When the thickness is increasingly thinned, the ferroelectric $\alpha\text{-In}_2\text{Se}_3$ can always maintain the IP and OOP polarization, regardless of thickness, and resists the impact of the depolarization field even at the atomic scale.

To better understand the dipole locking effect, Ding *et al.* employed the first-principle calculation²⁶ to predict the most effective kinetic pathway in the absence of an electric field [Fig. 3(a)]. The kinetics of polarization reversal between two stable states is associated with coordinated atom movement, which can be confined in three upper Se-In-Se layers with three stages. In the first stage, after overcoming the highest activation energy (0.066 eV), the atoms in three upper layers will move entirely along positive *a*-axis (see the small green arrows) and the $\alpha\text{-In}_2\text{Se}_3$ crystal transforms into a metastable structure. In the second stage, the central Se atoms rotate 60° around the C sites, giving rise to another degenerate structure [see the bottom schematic of Fig. 2(a)]. In the final stage, the In-Se atoms of the upper two-atom layers shift along the negative *a*-axis and rotate 60° away from the direction mentioned in the second stage. After the crystal transformation in these three stages, the OOP polarization reverses from downward to upward while the IP polarization simultaneously switches from [110] to [$\overline{1}\overline{1}0$]. Theoretical estimation also shows that in the presence of an IP and OOP electric field ranging from 0 to 0.3 V/ \AA , the corresponding activation energy slightly decreases by 0.003 and 0.01 eV, respectively, and the interlocked dipole can be fully toggled at 0.3 V/ \AA .

Having systematically elucidated the physics of the unique dipole locking effect, we now review the experimental breakthroughs that realized this novel mechanism. First, we examine the dipole locking effect in 3R structured $\alpha\text{-In}_2\text{Se}_3$. Xiao *et al.*³² used a second-harmonic generation (SHG) measurement, which is sensitive to probe the crystal's asymmetry,⁸⁸ to verify the concurrent dipole flipping across $\alpha\text{-In}_2\text{Se}_3$ at both IP and OOP directions.³² As shown in Fig. 3(b), SHG signals originating from the IP dipole of trilayer 3R $\alpha\text{-In}_2\text{Se}_3$ under normal incidence shows a strong response, in contrast with the signals from the substrate. After an OOP poling field is written into the sample in a square pattern (as marked by the dashed line), the corresponding OOP polarization can reverse, which is accompanied by the IP dipole flipping. As a result, dark lines occur at the boundary of the patterned area owing to destructive optical interference arising from the reversal of IP nonlinear optical polarization and the related IP lattice asymmetry. Such dark lines prove the unique dipole locking in two orthogonal IP and OOP directions. Second, we examine this effect in 2H-structured $\alpha\text{-In}_2\text{Se}_3$. Apart from the SHG measurement mentioned above, PFM can also be used to demonstrate the simultaneous flipping of IP and OOP ferroelectric polarization, which is done by using the twisting motions of the PFM probe at high frequency. Based on this technique, Xue *et al.* successively applied two kinds of OOP poling fields

with opposite directions into the two square patterns [Fig. 3(c)].³⁵ In response to such fields, both IP and OOP polarization reversals collected from a 2.3 nm-thick 2H $\alpha\text{-In}_2\text{Se}_3$ can be detected, as evidenced by the remarkable contrast in the PFM phase mapping.

The unique locking effect between IP dipoles and OOP dipoles offers another novel route to hold structural distortion at the atomic limit and accommodate the impact of the depolarization field. In principle, this regime is realized by the specific covalent bond configuration between the two inner In atom layers and central Se atom layer. In the OOP (or IP) direction, the structural instability, caused by the depolarization field, is counterbalanced or reduced by the IP (or OOP) covalent bonding. Such a neat OOP and IP locking effect therefore promises that monolayer ferroelectricity in $\alpha\text{-In}_2\text{Se}_3$ can survive at room temperature.³⁵ Meanwhile, the dipole locking also ensures the coexistence of OOP and IP piezoelectricity in 2H $\alpha\text{-In}_2\text{Se}_3$ at a thickness as thin as the monolayer (see Sec. III for details).⁸⁴ We stress that further progress can be made in the following directions. The polarization amplitude for both 2H and 3R $\alpha\text{-In}_2\text{Se}_3$ at various thicknesses is still unknown so far. The atomic visualization of dipole locking-based ferroelectric switching under an applied electric field has not yet been achieved. This may be atomically captured by high-resolution transmission electron microscopy with specific components. The gate-tunable ferroelectric switching is still ambiguous with respect to whether its origin results from the screening effect between domain walls and carriers or the switched ferroelectric domain (see Sec. II E for more details). The layer-dependent ferroelectricity in 2H $\alpha\text{-In}_2\text{Se}_3$ is currently under debate: from the view of structural analysis, the IP ferroelectricity in even layers will definitely be canceled out;⁸⁹ however, indeed the IP ferroelectric switching can be experimentally observed even in a multilayer. Furthermore, in the family of $\alpha\text{-In}_2\text{Se}_3$, the other ferroelectric compounds are also worthy of study. Special attention should be given to the identification of the crystal phase due to the ferroelectricity that exists in the 2H α phase, the 3R α phase and the β' phase.

C. Quadruple-well potential

In this section, we introduce the quadruple-well potential enabled by ion migration across the vdW gaps in the family of thio- and seleno-phosphate vdW ferroelectrics which represents another new ferroelectric property. As widely adopted by common ferroelectric systems,⁹⁰ the well-known double-well potential has two symmetrical energy minima that depict stable polarization states. Besides these two, Brehm *et al.* reported two additional symmetrical energy minima for thio- and seleno-phosphate vdW ferroelectrics.⁹¹ This is enabled by the presence of a stable position within vdW gaps for displacive metal ions. In total, there are four minima occurring in the potential energy curve: one pair with low polarization (LP) and the other pair with high polarization (HP), which are termed the quadruple-well potential.

The extensively studied vdW CuInP₂S₆ ferroelectric crystal^{24,25,40,50,51,91–97} is taken as an example to present a concrete interpretation of quadruple-well potential. With this new switching behavior, the CuInP₂S₆ switchable polarization has been confirmed at a thickness as thin as 4 nm (i.e., around 6 layers). We note that such 2D polarization can survive likely because the charged Cu ions move and approach the material interfaces under an applied electric field, and thus contribute to screening the depolarization field. We note that, in ferroelectric switching, this ion motion along *c* axis is entirely

different from that in oxide ferroelectrics where there is only a small shift from the center.

The relaxed crystal structure, for an equilibrium lattice constant (c lattice parameter) of 13.09 Å, is shown in Fig. 4(a), which usually concerns the two LP minima. In CuInP₂S₆, the Cu atom indicated by the blue ball is highly mobile along the z -axis and its displacement to equilibrium sites is responsible for the kinetics of intrinsic ferroelectric switching. When the metal Cu atom is electrically compelled to migrate across vdW gaps, as exhibited in Fig. 4(b), a stable Cu position is attained within the gaps and Cu forms new interlayer bonds with S atoms in the adjacent layers. This position commonly relates to the two HP minima. To better decipher the migration process, Brehm *et al.* employed first-principal calculation to investigate the possible kinetic pathway and energy barrier⁹¹ through displacing the Cu atoms to and beyond the equilibrium state [Fig. 4(c)]. The result reveals that under a c lattice constant of 13.09 Å, two LP states locating at the inner minima and two HP states residing at the outer minima, simultaneously occur in the energy vs polarization profile. Note that these four polarizations are all along the OOP direction, namely the z -axis. The inner local energy minimum in Fig. 4(c) corresponds to a Cu displacement of ~ 1.62 Å with polarization $P_{LP} = \pm 4.93 \mu\text{C cm}^{-2}$, while the outer minimum refers to a Cu-ion displacement of ~ 2.25 Å with polarization $P_{HP} = \pm 11.26 \mu\text{C cm}^{-2}$. Note that this outer energy minimum is essentially produced by the stable Cu position within the vdW gap, which extends the typical two polarization states ($\pm P_{LP}$) to four states and hence, represents a unique ferroelectric property. As shown by the potential profile in Fig. 4(c), the energy barrier between LP and HP is smaller than the thermal energy. Nevertheless, both polarizations can be stabilized at room temperature at a feasible c

lattice parameter or strain, which can be enforced by adjusting the scanning bias of the PFM probe.

The presence of quadruple-well potential can be corroborated by PFM measurement. In principle, due to their different structural distortions, the two crystal structure phases, including the Cu ion within and beyond vdW gaps, can produce different piezoresponses, which can be quantitatively probed by PFM. During measurement, CuInP₂S₆ crystal was transferred onto the In_{4/3}P₂S₆ substrate such that piezoelectric and non-piezoelectric responses could be conveniently identified. As shown in Fig. 4(d), there is a strong piezoresponse from ferroelectric CuInP₂S₆, which is in contrast with the nearly zero signal from In_{4/3}P₂S₆. The histogram of the piezoresponse extracted from Fig. 4(d) indicates four notable peaks [Fig. 4(e)] that fit well with the four polarization states in the potential well profile that were theoretically predicted [Fig. 4(c)]. From the histogram, a pair $16.6 \pm 0.8 \text{ pm V}^{-1}$ and $-11.8 \pm 1.3 \text{ pm V}^{-1}$ is identified as the positive and negative polarization states of the LP, while a pair $2.7 \pm 0.7 \text{ pm V}^{-1}$ and $2.9 \pm 1.0 \text{ pm V}^{-1}$ represents the two polarization states of HP. By contrast, the theoretical prediction of piezoelectric constants for LP is $-15.6 \pm 0.6 \text{ pm/V}$, whereas that for HP is $-2.5 \pm 0.7 \text{ pm/V}$. This consistency between experimental piezoelectric constants and theoretical estimation confirms the existence of four polarization states.

We also consider the following concomitant ferroelectric behaviors. Upon applying an electric field, the Cu ions can first move through intralayer and then into vdW gaps, leading to the polarization switching and the emergence of the quadruple-well potential. We remark that the quadruple well is strongly contingent on vdW gaps' ion migration and will presumably vanish at the monolayer limit. This makes it unclear whether monolayer CuInP₂S₆ retains polarization

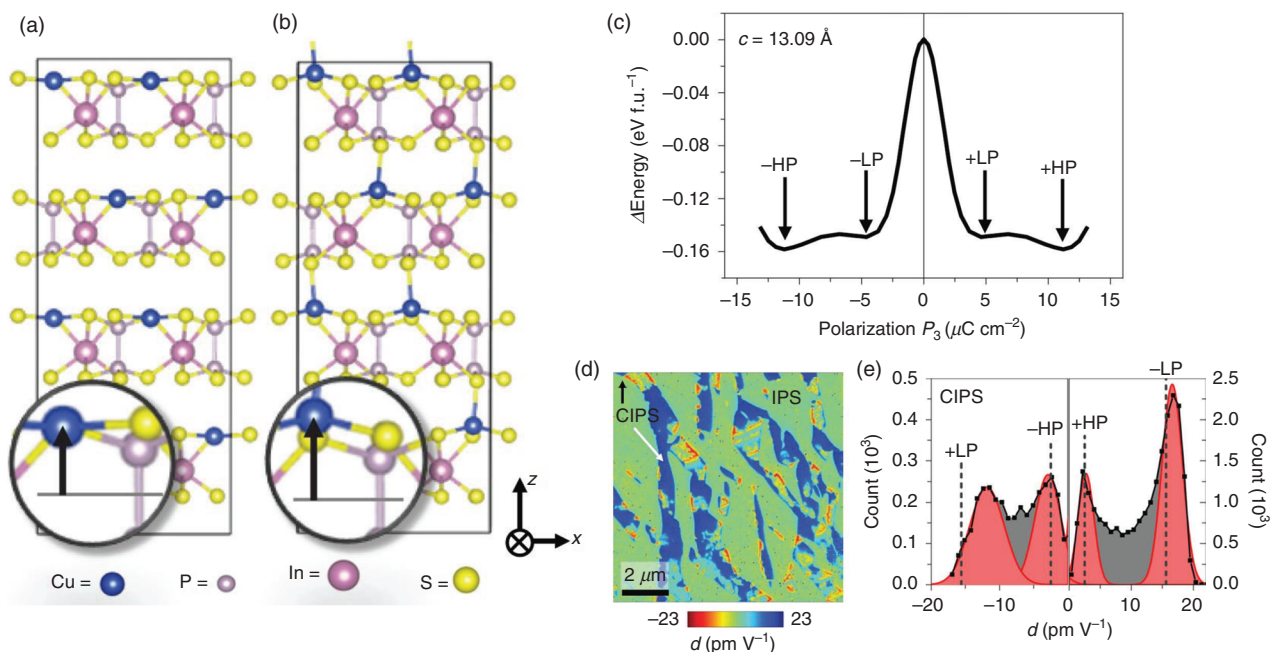


FIG. 4. Quadruple-well potential in vdW CuInP₂S₆. (a) and (b) Schematic crystal structures of CuInP₂S₆ for interpreting four polarization states. (c) Predicted potential well profile: energy vs polarization. (d) Quantitative piezoelectric constant mapping of CuInP₂S₆ flake. (e) Histogram of the extracted piezoelectric constant value from (d). The Gaussian function was used to fit the four distinct maxima. Reproduced with permission from Brehm *et al.*, Nat. Mater. **19**, 43, (2020). Copyright 2020 Springer Nature.⁹¹

switching. If it does, it is also unclear how the switching kinetics evolves compared to the aforementioned complex ferroelectric switching. Since the demonstrated thinnest thickness for CuInP₂S₆ ferroelectric is barely 4 nm, which corresponds to around 6 layers, the exploration of these confused points at the ultimate thickness will be extremely interesting. In addition, the following directions are albeit vital to elaborate the quadruple-well potential but are still unclear: (1) the impact of ion migration on tunnel transport in a ferroelectric tunnel junction across CuInP₂S₆ insulator (i.e., dynamic tunnel transport with respect to the Cu ion movement); (2) the effect of defects on the ion migration and quadruple-well potential; (3) the concrete behaviors of Cu ion at material interfaces (e.g., is there ion accumulation at one interface and ion deficiency at the other one?). Due to the ingeniously combined distinct properties—ferroelectric switching and ionic displacement—in vdW CuInP₂S₆, the study of this family of material may lead to the development of complex physics in pyroelectric, electrocaloric and thermal fields. It may also motivate novel and high-performance devices (see device Sec. III for more details).

Because of the emergence of the quadruple-well potential, some other new ferroelectric physics in CuInP₂S₆ have been discovered as well, for instance, negative piezoelectricity,⁹³ alignment of polarization against an electric field (i.e., inverse ferroelectric switching),⁹⁸ and negative slope of polarization vs electric field.⁹⁹ These three exotic phenomena all correlate with the Cu ion movement across the material's body. We note that the third effect can be elucidated by the explanations of

the second. Therefore, the negative piezoelectricity and inverse ferroelectric switching are discussed in detail in Secs. II C 1 and II C 2.

1. Giant negative piezoelectricity

Negative piezoelectric materials feature contraction responses when an electric field is applied along the polarization direction, which are different from elongation responses in common positive piezoelectric materials. These types of materials are quite scarce. For a long time, the only experimentally explored material was ferroelectric polymer poly (vinylidene fluoride) (PVDF) and its copolymers. With the extensive studies on vdW ferroelectrics, another class of negative piezoelectrics is found in thio- and seleno-phosphate ferroelectrics in 2019,⁹³ i.e., CuInP₂S₆, which is essentially enabled by strain-tunable, quadruple-well potential.⁹¹

We first look into the underlying mechanism of unique negative piezoelectricity using stress-tunable potential curves. Brehm *et al.* predicted that the exotic CuInP₂S₆ potential landscape can be dramatically tuned by changing *c*-lattice parameter [Fig. 5(a)], which is equivalent to macroscopically applying stress.⁹¹ At a smaller *c*-lattice (i.e., compressive stress), the +LP energy minima will disappear while at a larger *c*-lattice (i.e., tensile stress) it is the +HP minima that will vanish. One can also see that, through varying the *c*-lattice, the quadruple-well potential in vdW CuInP₂S₆ is able to transform into double-well potential [Fig. 5(a)], indicating that polarization values

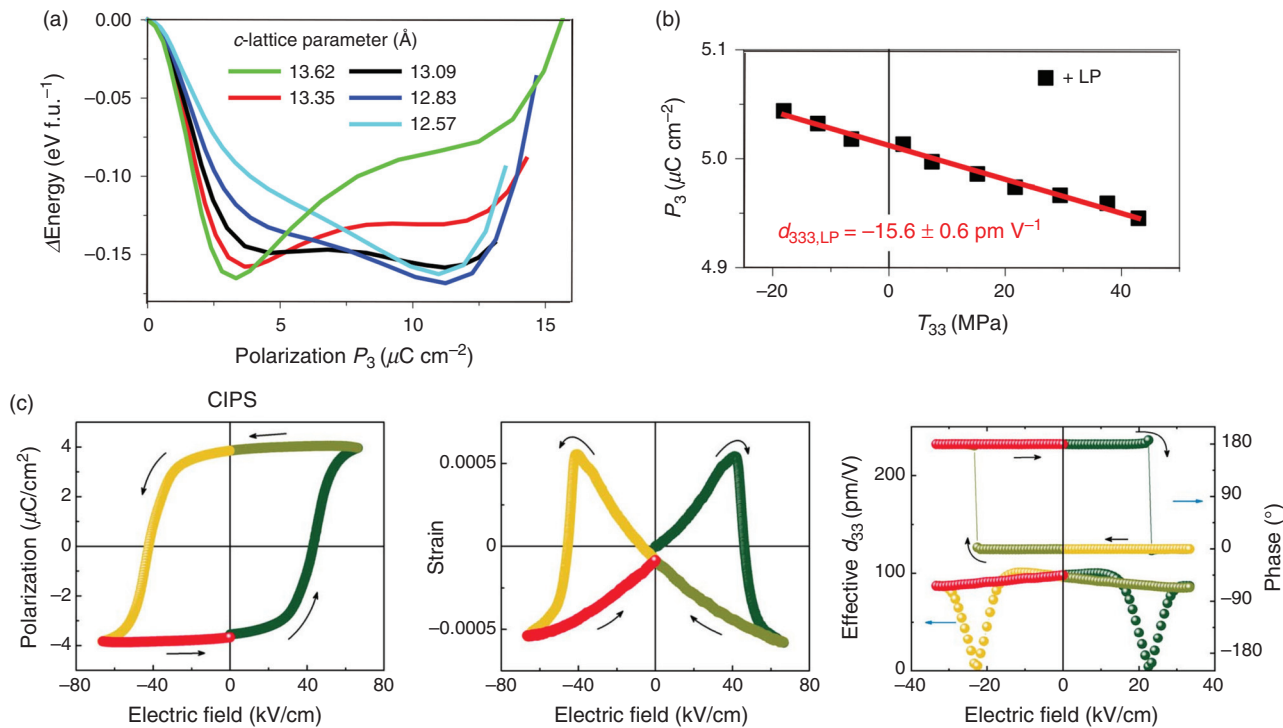


FIG. 5. Giant negative piezoelectricity in vdW CuInP₂S₆. (a) The predicted lattice-parameter-dependent (i.e., strain) potential landscape in the case of positive polarization. The polarization is estimated along the *c* axis. The equilibrium of *c*-lattice is 13.09 Å. (b) Theoretical polarization values as a function of stress for +LP state. The stress is applied along the *z* axis of CuInP₂S₆. Reproduced with permission from Brehm *et al.*, Nat. Mater. **19**, 43 (2020). Copyright 2020 Springer Nature.⁹¹ (c) Hysteresis loops of polarization-electric field, strain-electric field, and d_{33} -electric field of CuInP₂S₆. Reproduced with permission from You *et al.*, Sci. Adv. **5**, eaav3780 (2019). Copyright 2019 American Association for the Advancement of Science.

located at potential minima are contingent on c -parameter or stress. To quantitatively present their underlying relationships, Brehm *et al.* calculated the +LP polarization values as a function of applied stress⁹¹ as shown in Fig. 5(b). At around zero stress, the linear fit of polarization values vs stress can be used to precisely deduce piezoelectric coefficient, according to $d_{kij} = \partial P_k / \partial T_{ij}$. The negative correlation between P_k and T_{ij} reveals that CuInP₂S₆ possesses an abnormally negative piezoelectric coefficient (i.e., -15.6 ± 0.6 pm/V). In conclusion, from a theoretical perspective, this unique property originates from the vdW stacking and Cu ion migration, as evidenced by the formation of multiple-well potential via Cu ion migration in Fig. 4 and by the strain tunability.

You *et al.* have experimentally probed such a negative piezoresponse effect using a set of PFM hysteresis loops such as polarization vs electric field, strain vs electric field, and d_{33} vs electric field.⁹³ We note that, although You *et al.* also provided a theoretical interpretation for this effect, the calculation from Brehm and coauthors seems more convincing. As shown in Fig. 5(c), when an electric field increases from zero to its positive maximum (i.e., stage 1), the polarization of CuInP₂S₆ is incrementally aligned to the same direction with the electric field, and consequently changes from a negative value to a positive one. Meanwhile, the electric-field-induced strain almost linearly increases, reaches a peak at the coercive bias, and finally decreases to a negative maximum. Accordingly, CuInP₂S₆ expands at a small electric field and further contracts at a large field that exceeds the coercive field. As the electric field decreases from the positive maximum to zero (i.e., stage 2), polarization can be stably maintained but the strain linearly drops to zero. These electromechanical characteristics in stages 1 and 2 indicate that CuInP₂S₆ is a negative piezoelectric material and its estimated piezoelectric coefficient is as high as -95 pm/V [the right panel of Fig. 5(c)].

Neumayer *et al.* affirmed that, in addition to the giant negative piezoelectricity, CuInP₂S₆ also shows a great negative electrostriction of $-3.2 \text{ m}^4/\text{C}^2$.³⁸ This value is roughly 100 times larger than that in well-established lead zirconate titanate. More interestingly, such a unique negative electrostriction can be maintained even at a paraelectric state above Curie temperature. The combined giant negative piezoelectricity and great negative electrostriction make CuInP₂S₆ highly promising for fabricating flexible high-performance electromechanical devices. We note that, aside from inverse piezoelectric response, the electrostriction is the other electromechanical response when an electric field is applied; electrostriction response is proportional to the square of electric field while inverse piezoelectric response maintains linearity with the electric field. Even though electrostriction in part relates to the negative piezoelectric responses in CuInP₂S₆, the mechanism of unusual electrostriction properties deserves further exploration.

2. Inverse polarization switching

In contrast with common positive polarization switching, we define inverse polarization switching as polarization alignment against the direction of an applied electric field. This unique, interesting phenomenon was first discovered by Neumayer *et al.* in CuInP₂S₆. It has the same origin⁹⁸ as the quadruple-well potential mentioned in Fig. 4: a synthesis result of Cu ion unidirectional migration across vdW gaps, unlike the dipole reorientation in other ferroelectrics.

Neumayer *et al.* used a negative pulse train with different widths to pole a CuInP₂S₆ flake whose initial polarization points downward.⁹⁸ By systematically analyzing the corresponding piezoresponses, an abnormal polarization transition was identified [see Fig. 6(a)]. At the first state (i.e., the duration below 0.7 s), CuInP₂S₆ polarization is expectedly aligned with the electric field from -LP to +LP, and then to +HP. However, at the second state (i.e., duration exceeding 0.7 s), the polarization shows an abrupt transition from +HP to -HP, which is surprisingly against the orientation of applied electric field and contradicts the polarization-switching mechanism in other reported ferroelectrics. The change in polarization direction under an applied electric field can also be used to explain the negative slope of polarization vs electric field ($\frac{\partial P}{\partial E} < 0$ where P and E are polarization and electric field, respectively), which is a third unusual switching effect of CuInP₂S₆. This effect represents a new finding for accessing negative capacitance to overcome Boltzmann limit for energy-efficient uses. If one is interested in the negative capacitance development, Iniguez and coauthors' review article is a good source.¹⁷ Now, we return to the third state (i.e., duration exceeding 0.9 s) in Fig. 6(a): the CuInP₂S₆ polarization switches back to +LP and is realigned to the same orientation with the applied electric field. Obviously, by using unipolar poling pulses with fixed amplitudes but different widths, the change in polarization orientation is enabled, during which the inverse ferroelectric switching occurs.

As shown in Fig. 6(b), the inverse polarization switching can be vividly depicted as the Cu ion movement across vdW intralayers and gaps. Remarkably when the electric field compels Cu ions to move upward, the polarization transition between four states (-LP, +LP, -HP, and +HP) strongly depends on the Cu ion position. The -LP and +LP states are associated with the Cu location within intralayers, whereas +HP and -HP states correspond to the position within vdW gaps. Under an upward electric field, the transition from +HP to -HP leads to the inverse ferroelectric switching. To provide further insight into the Cu displacement, Neumayer *et al.* also plotted a schematic trajectory to clearly present Cu positions with respect to polarization states [Fig. 6(c)]. The Cu ions have a unidirectional migration that periodically crosses vdW layers and gaps, resulting in the abnormal polarization transition in Fig. 6 and the quadruple-well potential mentioned in Fig. 4.

The inverse ferroelectric switching features a unipolar poling voltage, unlike the bipolar voltages used for common ferroelectric switching. Together with multilevel polarization states, it will provide new opportunities for ferroelectric memories with high-density data storage and low-power consumption.

D. Piezoelectric domain walls

We now consider an unusual domain walls—piezoelectric domain walls in polar vdW materials. These walls are a new domain structure over which special boundaries separate polar and nonpolar domains with different piezoresponses. Dziaugys *et al.* investigated this unique physical phenomenon in vdW antiferroelectric CuInP₂Se₆, which belongs to the family of thio- and seleno-phosphate vdW ferroelectrics.⁵⁶ They found that the piezoelectric domain walls exhibit the strongest piezoresponses, an up to fourfold enhancement over what is found within domains. The authors attributed this phenomenon to the coexistence of nonpolarized antiferroelectric and polarized ferroelectric phases.

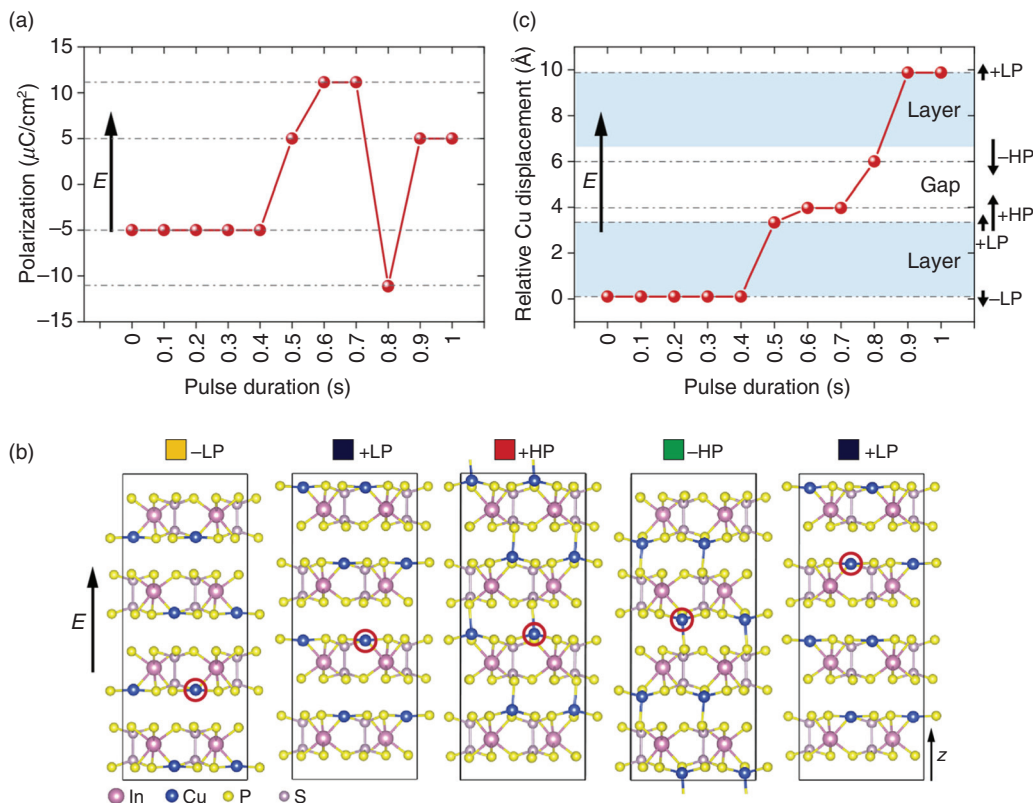


FIG. 6. Inverse polarization switching in vdW CuInP_2S_6 . (a) Polarization with respect to applied pulse duration. The back arrow indicates the direction of applied electric field. (b) Schematics of structural evolution for the switching pathway in (a). The red circles show the exact atom position switched by applied electric field. (c) Relative Cu displacement with respect to applied pulse duration for the pathway in (a). The intralayer, vdW gap, and polarization change are highlighted. Reproduced with permission from Neumayer *et al.*, Phys. Rev. Appl. 13, 064063 (2020). Copyright 2020 American Physical Society.⁹⁸

To investigate this unique domain wall in $\text{CuInP}_2\text{Se}_6$, the measurement temperature was cooled to 140 K. Figures 7(a) and 7(c) show significant piezoresponses: the irregular boundaries divide piezoresponse mapping into two different regions; the ferroelectric phase shows a greater piezoresponse over the antiferroelectric phase; the greatest piezoresponse comes from the irregular boundaries. For comparison, Dziaugys *et al.*⁵⁶ examined the piezoresponses of CuInP_2S_6 as indicated in Figs. 7(b) and 7(d). By contrast, the domain boundaries in CuInP_2S_6 show a near zero piezoresponse and their adjacent domains have opposite piezoresponses with almost the same amplitude. These findings confirm that the piezoelectric domain walls in $\text{CuInP}_2\text{Se}_6$ exist and separate disparate ordering regions. Moreover, the authors also demonstrated that an electric field applied onto PFM probes can markedly modulate the piezoresponses of these walls, and what's more, the strong responses can disappear through the application of a negative probe voltage.

This type of domain wall enriches our understanding of topological structures in polar ferroelectrics. The neat coexistence of ferroelectric and antiferroelectric phases in $\text{CuInP}_2\text{Se}_6$ demonstrates that non-polar materials can be artificially designed and engineered with localized polar regions and vdW heterostructures can be functionalized. We note that Dziaugys *et al.* made the first step toward unveiling this new domain structure. Nevertheless, to adequately decipher it, much

work remains to be done. For example, the regime of piezoelectric domain walls with ferroelectric and antiferroelectric phases split into different regions is still not well understood. Its stabilization is particularly fascinating due to the instability caused by the fact that: one side of the wall has no charges but the other side carries polarization charges. Additionally, the disappearance of domain wall piezoresponse enabled by a negative voltage suggests that this new piezoelectric wall can also be written or erased in the same way as the ferroelectric walls, and thus, it is a new entity for constructing domain wall electronics.

E. Gate-tunable polarization

The next fascinating property that we examine in vdW's ferroelectrics is gate-tunable polarization. This is essentially created by the semiconducting characteristic of several vdW ferroelectrics, such as $\alpha\text{-In}_2\text{Se}_3$ and SnS, and their transistor architectures. The gate tunability is unprecedented and non-trivial in the ferroelectric realm. On one hand, its implementation in oxide ferroelectrics, such as BaTiO_3 and PZT, presents huge challenges due to the large bandgaps and low conductivities. On the other hand, it allows for the manipulation of structural asymmetry to further control over ferroelectricity.

Xue *et al.* first demonstrated gate-tunable polarization in semiconducting $\alpha\text{-In}_2\text{Se}_3$ ferroelectric.⁵⁷ As seen in the gate-tunable I-V

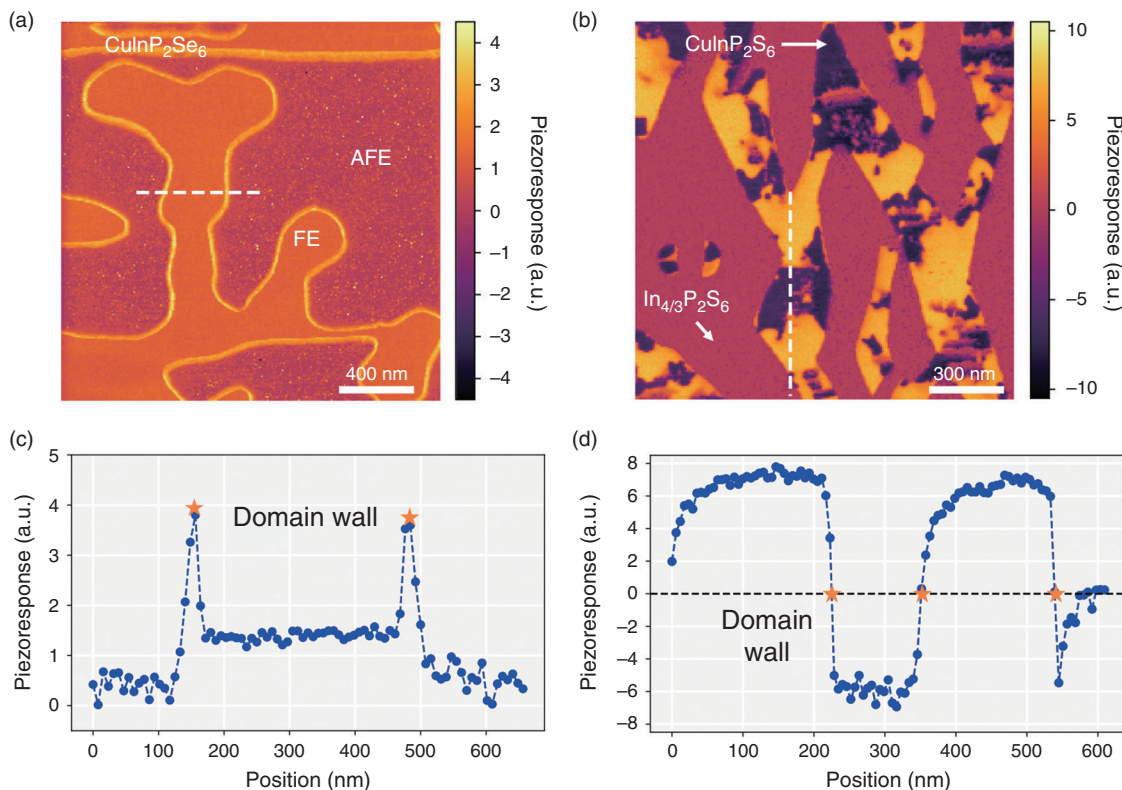


FIG. 7. Piezoelectric domain walls in vdW $\text{CulnP}_2\text{Se}_6$. (a) $\text{CulnP}_2\text{Se}_6$ piezoresponse mapping for the signal $\text{Acos}(\theta)$ (A and θ dictate amplitude and phase, respectively). For comparison, CulnP_2S_6 piezoresponse mapping is also shown in (b). Note that the data in (a) were collected at 140 K in ultrahigh vacuum while that in (b) obtained at room temperature in a special environment. (c) and (d) The corresponding profiles of piezoresponse signals extracted from the white dashed lines in (a) and (b). Reproduced with permission from Dziaugys *et al.*, Nat. Commun. 11, 3623 (2020). Copyright 2020 Springer Nature.⁵⁶

curves in Fig. 8(a), a gate field between the back gate and the grounded source terminal can open or close switching windows. This suggests that the polarization of $\alpha\text{-In}_2\text{Se}_3$ channel can be flipped by gate biases, given that the charger trapping effect has been ruled out in planar $\alpha\text{-In}_2\text{Se}_3$ devices. With the decrease in gate biases, the switching windows are markedly enlarged, signifying an increase in polarization magnitude across the $\alpha\text{-In}_2\text{Se}_3$ channel. We note that this gate tunability detected by electrical measurement indeed involves complex ferroelectric physics, for example, carrier injection by back gates, domain switching underneath the grounded electrode, and source-drain Schottky barrier change. Therefore, its exact underlying mechanism in $\alpha\text{-In}_2\text{Se}_3$ needs experimental clarification, using, for example, *in situ* PFM measurements.

Bao *et al.* utilized SHG measurement to unambiguously find that intrinsic centrosymmetry breaking is responsible for gate-tunable switching windows in semiconducting SnS ferroelectric.⁴³ They fabricated a lateral few-layer-SnS device on silica wafers and observed remarkable hysteresis [see Fig. 8(b)], a signature of ferroelectricity. They also conducted I-V hysteresis loops as a function of gate biases, from which P-E loops were derived with the equation $P = \frac{\int IdV}{sv}$ where I , V , s , and v indicate current, voltage, effective area, and scanning velocity, respectively [see Fig. 8(c)]. As the gate bias is lowered,

particularly to a negative value, the P-E switching windows grow remarkably [Fig. 8(c)]. To account for this gate-tunable polarization, SHG measurement was employed to probe crystal asymmetry with regard to gate biases. As revealed in Fig. 8(d), a negative gate bias can displace off-centered ions farther from the equilibrium sites and induces stronger dipoles (SHG intensity) than a positive gate voltage.

The gate tunability of ferroelectric polarization can create an opportunity for systematically studying the interplay between ferroelectric instability, topological structures, and free carriers, which have not yet been addressed so far in oxide ferroelectrics. We believe that, by injecting free carriers into ferroelectrics, the ferroelectric domain walls could be manipulated due to the disturbed screening effect of polarization charges at domain walls. This manipulation method may offer a new degree of freedom in engineering ferroelectric domain walls apart from electrical and optical methods.

III. NOVEL FERROELECTRIC DEVICES

In this section, we talk about novel and advanced devices for information storage and energy harvesting enabled by the unique vdW ferroelectric properties. These innovative devices incorporate new technologies for constructing devices that, thus far, have had difficulty using oxide ferroelectrics.

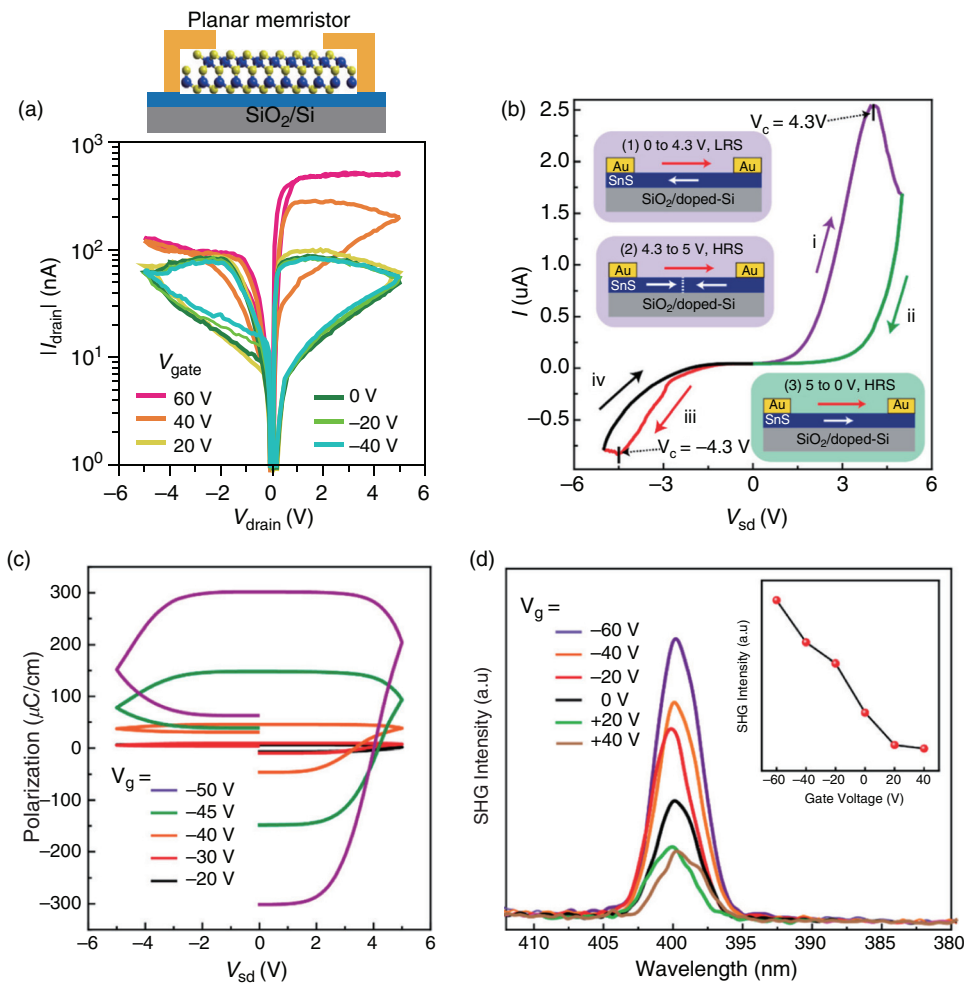


FIG. 8. Gate-tunable polarization in vdW In_2Se_3 and SnS. (a) Pinched hysteresis loops tuned by different gate biases for an α - In_2Se_3 device. The top shows an α - In_2Se_3 device sketch. Reproduced with permission from Xue *et al.*, *Adv. Mater.* **31**, 1901300 (2019). Copyright 2019 Wiley-VCH.⁵⁷ (b) Pinched hysteresis loops of a SnS device. (c) P-V hysteresis loops under different gate biases for a lateral SnS ferroelectric device. (d) SHG intensity as a function of gate biases. Reproduced with permission from Bao *et al.*, *Nano Lett.* **19**, 5109 (2019). Copyright 2019 American Chemical Society.⁴³

A. Multidirectional switchable memristors

The dipole locking effect fundamentally enables IP pulse programming of OOP resistance switching and OOP pulse programming of IP resistance switching, which can be described with the term “multidirection-switchable memristive phenomena.” Xue *et al.* demonstrated these phenomena using a delicate device structure,⁵⁷ composed of an α - In_2Se_3 fake sandwiched by predefined source-drain electrodes at the bottom and circular electrodes at the top [Fig. 9(a)]. As shown in Fig. 9(b), after applying an IP programming pulse on source-drain terminals, the OOP electrical IV curves exhibit remarkable current switching. Meanwhile, the OOP programming pulse also affects the IP current switching [Fig. 9(c)]. At the α - In_2Se_3 device level, an IP (or OOP) poling pulse can reverse the corresponding IP (or OOP) polarization, leading to IP (OOP) resistance switching; simultaneously, in the normal direction, the related OOP (or IP) polarization and resistance can also be switched due to the dipole locking effect.

Prototype nanoscale memory devices, which are based on either OOP polarization or IP polarization of ferroelectric α - In_2Se_3 , have shown potential for high-density information storage in the post-Moore era. When these α - In_2Se_3 memory devices are densely

integrated, on the one hand the multi-direction-switchable memristive phenomena provide a new avenue for adjusting and further decreasing device variations within the array; on the other hand, they are also expected to help significantly reduce peripheral circuitry through multiterminal design. Note that even although the multiterminal design inevitably decreases integration density, cumbersome peripheral circuitry in a conventional memristor array also hampers attempts to increase the three-dimensional monolithic integration density. Therefore, to implement the strength of multidirectional switchable memristive phenomena, we believe that a trade-off between multiterminal design and integration density will remain in future vdW ferroelectric memristors.

B. Optoelectronic ferroelectric memories

Optically controlled ferroelectric polarization in vdW α - In_2Se_3 can be used to store and retrieve light information and to achieve optoelectronic ferroelectric memories by using only a single ferroelectric. These unprecedented memories feature simplified device structures,⁵⁸ i.e., a single ferroelectric bridging two electrode terminals, compared to other similar devices based on vdW materials.^{100–102} The

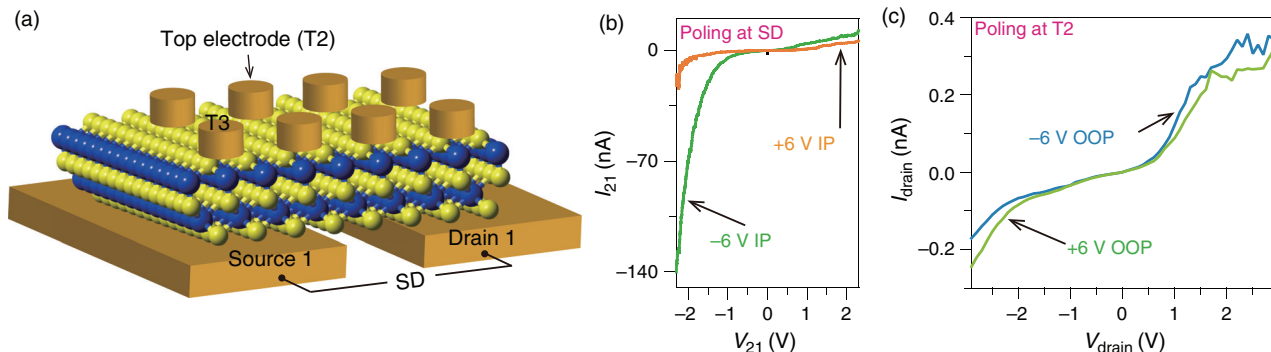


FIG. 9. Multidirectional switchable memristive phenomenon (a) Schematic of the device structure. The electrodes are composed of bottom source-drain stripe metal and top circular metal. (b) OOP current (resistance) switching measured from terminal T2-Source1. The switching results from IP source-drain poling. During measurement, the source and drain are grounded. (c) IP current switching triggered by OOP pulse poling. The small-area switched domain by OOP biases leads to the small current change in IV curves. Reproduced with permission from Xue *et al.*, *Adv. Mater.* **31**, 1901300 (2019). Copyright 2019 Wiley-VCH.⁵⁷

successful implementation of such novel ferroelectric memories in vdW α -In₂Se₃, rather than in conventional oxide ferroelectrics, is ascribed to the ingenious combination of superior semiconduction, excellent optical properties, and stable polarization in a single ferroelectric α -In₂Se₃.

Xue *et al.* demonstrated prototypical optoelectronic ferroelectric memories by using a photocurrent-driven domain wall, which marked the first attempt to technologically apply optically controlled ferroelectric polarization in device application.⁵⁸ In Fig. 10(a), the enclosed area shown with white dashed lines indicates the α -In₂Se₃ channel, which connects the T3 terminal and T4 terminal. After the application of -4 V poling voltage onto T3, a ferroelectric domain wall is created across the channel [Fig. 10(b)]. Interestingly, upon being illuminated by light, this domain wall moves toward the T3 terminal, whereas the light is removed, it stabilizes at a position in a nonvolatile manner [see Fig. 10(c)], which is favorable for light information storage. Subsequently, when a $+4$ V poling voltage is applied, the ferroelectric domain wall can be fully erased [Fig. 10(d)]. Notably, after light irradiation, this domain wall in α -In₂Se₃ is reconfigurable, movable, and erasable. Meanwhile, with the same experimental conditions, the time-resolved current was collected from the device as shown in Fig. 10(a) to characterize device electrical properties [Fig. 10(e)]. The nonvolatile photoresponse shown in Fig. 10(e) and *in situ* PFM results in Figs. 10(b)–10(d) demonstrates the capability of optically storing and electrically erasing light information in ferroelectric domain walls. The underlying mechanism can be attributed to the disturbed screening to domain walls by photogenerated carriers.⁵⁸

Two-terminal optoelectronic ferroelectric memory represents the first progress to use ferroelectric domain walls to store light information, which is realized in a nonvolatile manner through photocurrent-driven domain walls. This device has a simplified structure and shows promise for uses in constructing device arrays for neuromorphic vision sensors and image recognition. Along these lines, the device's optical writing time needs to be optimized toward a nanosecond scale, which can likely be done by using quantum dots adorned on α -In₂Se₃ surfaces to enhance light absorption. Another fascinating line is to achieve photonic in-memory computing chips that physically combine light sensing, logic, and memory functionalities. We note that the commercialized mainstream optoelectronic memories are based on silicon but

have separate sensing and memory cells which inevitably results in energy consumption and decreased speed due to the data shuttling between these two parts. However, photonic chips based on this new technology could overcome these issues.

C. Ferroelectric semiconductor transistors

The new type of ferroelectric semiconductor transistors proposed by Si *et al.*⁴⁷ feature a semiconducting ferroelectric as a channel material. Unlike conventional ferroelectric transistors that use insulating ferroelectrics with a poor dielectric property as gate dielectrics¹⁰³ [Fig. 11(a)], the novel ferroelectric semiconductor transistors enable the use of high-quality amorphous gate insulators, which potentially eliminates gate-leakage currents. As shown in the right panel of Fig. 11(a), the polarization switching upon applying a large gate-source electric field can trigger hysteresis in channel conductivity through modulating interface Schottky barriers. We emphasize that successfully developing such a novel ferroelectric device would benefit from a material incorporating a semiconducting property and stable ferroelectric polarization in a material.

Si *et al.* employed ferroelectric α -In₂Se₃ to demonstrate ferroelectric semiconductor transistors.⁴⁷ A layer of Al₂O₃ was grown on the device by atomic-layer-deposition at low temperature to prevent α -In₂Se₃ surface degradation. As exhibited in Fig. 11(b), a marked hysteresis is observed as the gate voltages sweep back and forth. More importantly, the obtained I_D-V_{GS} curves reveal the high performance of α -In₂Se₃ ferroelectric semiconductor transistors: a high on/off ratio of over 10⁸ read at V_{DS} = 1 V and a high extracted field-effect mobility of 312 cm² V⁻¹ s⁻¹ in forward scan and 488 cm² V⁻¹ s⁻¹ in reverse scan. Output I_D-V_{DS} curves [Fig. 11(c)] demonstrate a maximum drain current of 671 μ A μ m⁻¹, applicable for high-speed electronic application. In addition, Wang *et al.* reported the application of α -In₂Se₃ ferroelectric semiconductor transistors in neuromorphic computing⁸³ as shown in Fig. 11(d). An electrical spike was applied onto the gate and synaptic connectivity was emulated by the change in ferroelectric channel conductivity. With the firing of identical pulses, the α -In₂Se₃ device shows periodic potentiation and depression.

This ferroelectric semiconductor transistor sidesteps the use of oxide ferroelectrics as gate dielectrics which usually have poor

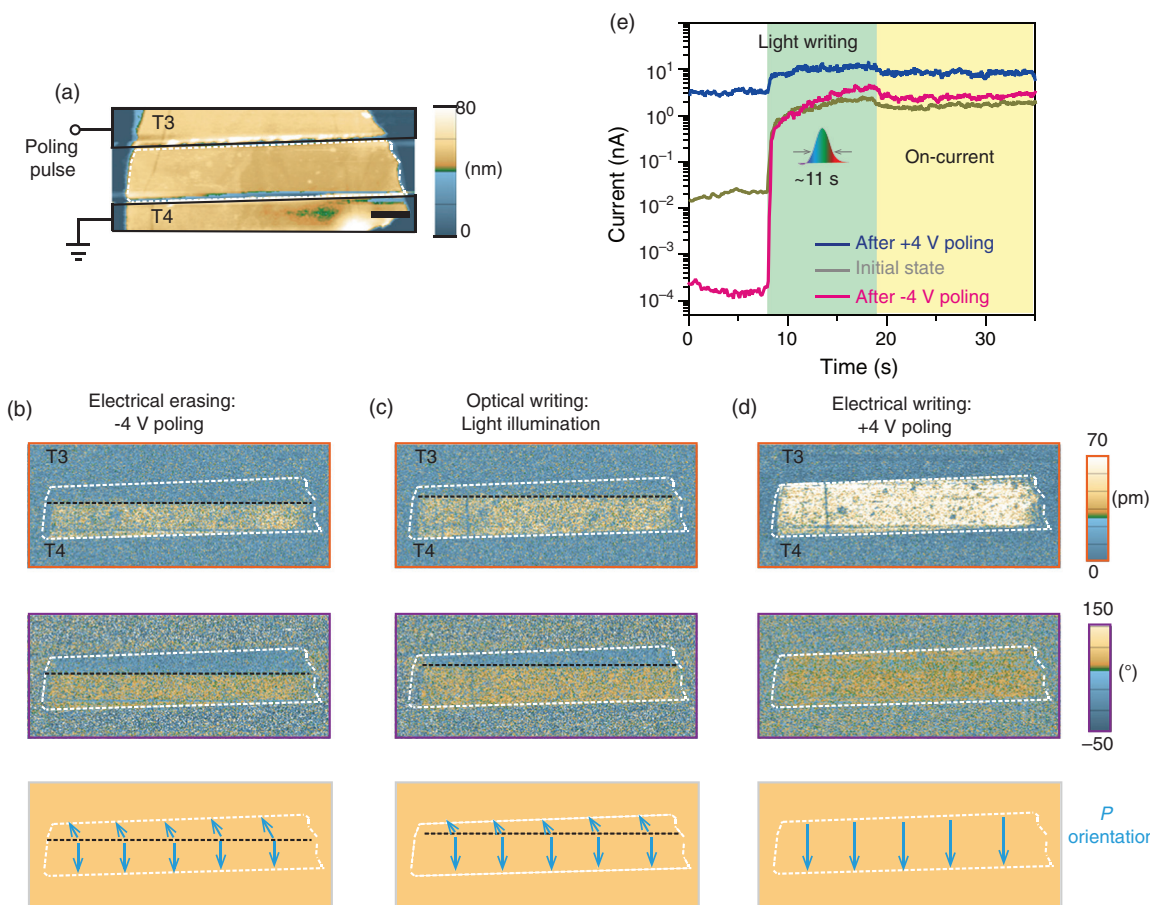


FIG. 10. Optoelectronic ferroelectric memories. (a) AFM topography of the used α -In₂Se₃ device. The poling pulses are applied onto T3 terminal. PFM study and interpretation of ferroelectric domain wall evolution under different experimental conditions: (b) after -4 V poling, (c) after -4 V poling and subsequent light illumination, (d) after $+4$ V poling. (e) Drain-source currents with electrical poling and light illumination. Reproduced with permission from Xue *et al.*, *Adv. Funct. Mater.* **28**, 1803738 (2020). Copyright 2020 Wiley-VCH.⁵⁸

dielectric properties, but directly utilize semiconducting vdW ferroelectrics as channel materials. This new device should therefore reduce the large leakage currents and the influence of interfacial charges on polarization stability, which often deteriorates retention performance for traditional ferroelectric field-effect transistors. Further lines can proceed along the large-scale integration of these new devices for complex computation.

D. VdW ferroelectric heterostructure-based devices

VdW ferroelectrics are essentially free from dangling bonds and are easy to be artificially assembled with other dissimilar materials without considering lattice matching. These characteristics enable the realization of novel, low-dimensional, high-performance, heterostructure-based devices. Combining vdW ferroelectric insulators (e.g., CuInP₂S₆) with high-mobility 2D materials (e.g., MoS₂) can create purely 2D heterostructure transistors and memories^{44,51,95,104} [see Fig. 12(a)], that are distinct from 2D–3D hybrid transistor devices in terms of architecture.^{103,105} Si *et al.* were the first to implement this device concept to achieve a vdW ferroelectric heterostructure-based

transistor for memory applications,⁵¹ whose I_D-V_{TG} hysteretic curves are presented in Fig. 12(b). We note that the demonstrated performances of, for example, on/off ratio and subthreshold swing are not competitive and leave much room for improvement.

Later, Wang *et al.* achieved vdW ferroelectric heterostructure-based negative capacitance transistors showing high performances mainly for logic applications.¹⁰⁴ They noted that a top gate, constructed by a vdW ferroelectric heterostructure, can reduce gate-leakage currents due to its ideal insulator-semiconductor interface and further enhance on/off ratio. As shown by the top-gate biases vs drain-source currents in Fig. 12(c), the transition between off-current and on-current is steep, particularly in the reverse sweep, resulting in a subthermionic value. The minima can reach 39 and 28 mV dec⁻¹ for both forward and reverse sweeps, respectively [see Fig. 12(d)]. By optimizing dielectric thickness and ferroelectric capacitance, the hysteresis in Fig. 12(c) is largely suppressed even to zero and the subthreshold swing is greatly decreased as well, constituting an ideal hardware for logic operations.

In addition, Wu *et al.* also demonstrated a ferroelectric tunnel junction by using vdW ferroelectric heterostructures,¹⁰⁶ i.e., CuInP₂S₆

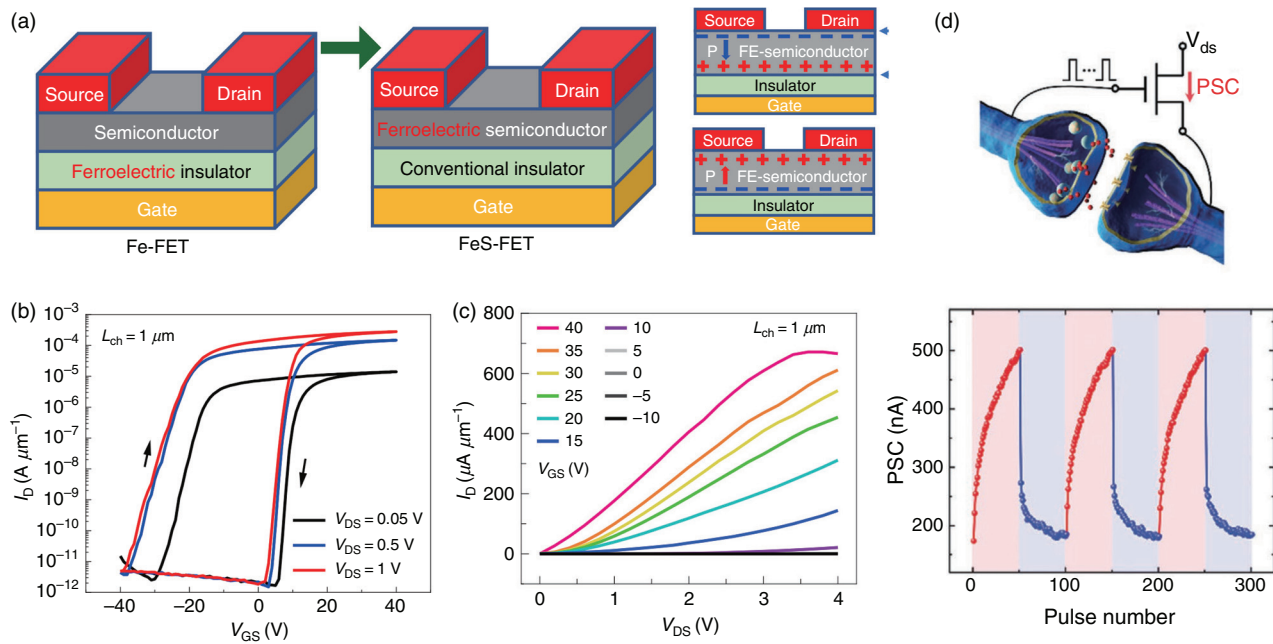


FIG. 11. Ferroelectric semiconductor transistors. (a) Schematic illustrations of ferroelectric transistor (Fe-FET) and ferroelectric semiconductor transistor (FeS-FET). The right panel shows polarization bound charge distribution under different poling conditions. (b) Hysteretic I_D - V_{GS} transfer curves. (c) I_D - V_{GS} output curves. Reproduced with permission from Si *et al.*, Nat. Electron. **2**, 580 (2020). Copyright 2020 Springer Nature.⁴⁷ (d) Schematic of a solid-state synapse emulated by a ferroelectric semiconductor transistor (top panel) and potential and depression responses with identical pulses. Reproduced with permission from Wang *et al.*, Adv. Funct. Mater. **30**, 2004609 (2020). Copyright 2020 Wiley-VCH.⁸³

and graphene stacking [see Fig. 12(e)]. In these devices, graphene and Cr act as a bottom electrode and a top electrode, respectively, for sandwiching ferroelectric CuInP₂S₆. Such a configuration forms asymmetric Schottky barriers, through which ferroelectric switching can effectively modulate tunnel electroresistance and attain a value of over 10^7 [see Fig. 12(f)].

The 2D ferroelectric heterostructures are stacked by assembling disparate 2D materials but retain at least one ferroelectric sheet. Since 2D materials encompass rich properties including semimetallicity, insulativity, ferroelectricity, ferromagneticity, and superconductivity, these diversities provide a functional reservoir for building strongly correlated ferroelectric interfaces where, for example, by amplifying gate biases, ferroelectric switching allows the negative capacitance to be accessed for low-power transistors; via Schottky barrier modulation, ferroelectric switching enables the giant electroresistance of high-performance tunnel junctions. Furthermore, these vdW ferroelectric interfaces are also promising for spintronic devices: through the proximity effect, ferroelectric switching can control over ferromagnetism and further achieve nonvolatile electric-field-modulated ferromagnetic switching.

E. Piezoelectric nanogenerators with flexible design

Xue *et al.* demonstrated that the dipole locking effect bestows vdW α -In₂Se₃ ferroelectric with piezoelectricity in both IP and OOP directions, irrespective of sample thickness⁸⁴ [Figs. 13(a) and 13(b)]. Such unique piezoelectric characteristics are more practical compared to the piezoelectricity in the transition metal dichalcogenides

(TMDCs) family and BN, which is solely confined to the IP direction and is dependent on sample thickness (the piezoelectricity exists in an odd layer but vanishes in an even layer; with an increase in thickness, the piezoelectric constant decreases and finally vanishes).⁶⁰ If constructing nanoscale piezoelectric devices, such as piezoelectric nanogenerators and piezotronic devices, it will be more flexible and simple to deposit metal electrodes on α -In₂Se₃ without identifying the sample thickness and considering the polarization direction. As indicated in Figs. 13(c) and 13(d), an α -In₂Se₃ piezoelectric nanogenerator can be facilely acquired following two steps: first, a stochastic-thickness flake exfoliated from the parent crystal is transferred onto a PE substrate; second, metal electrodes are flexibly made to form electrical contact with the piezoelectric material. Upon applying a periodic strain, the corresponding piezoelectric outputs with alternative current [Fig. 13(e)] are obtained because of the modulation of the Schottky barrier height on the metal-semiconductor interface by piezoelectric polarization charges. More importantly, the coupling of IP and OOP piezoelectricity guarantees that under any strain direction, there will always be piezoelectric outputs (see outputs along x and y directions for reference). Additionally, Dai *et al.* reported that the rhombohedral α -In₂Se₃ ferroelectric, distinct from hexagonal α -In₂Se₃ used in Figs. 13(a)-13(e), is also capable of flexibly creating piezoelectric devices regardless of sample thicknesses¹⁰⁷ [Figs. 13(f)-13(h)].

The dipole locking effect in α -In₂Se₃ favors the existence of IP and OOP piezoelectricity at any thickness. This allows us to flexibly construct piezoelectric nanogenerators and ignore the polar axis and sample thickness which must be considered when fabricating 2D-materials-based energy-harvesting cells. We note that further studies

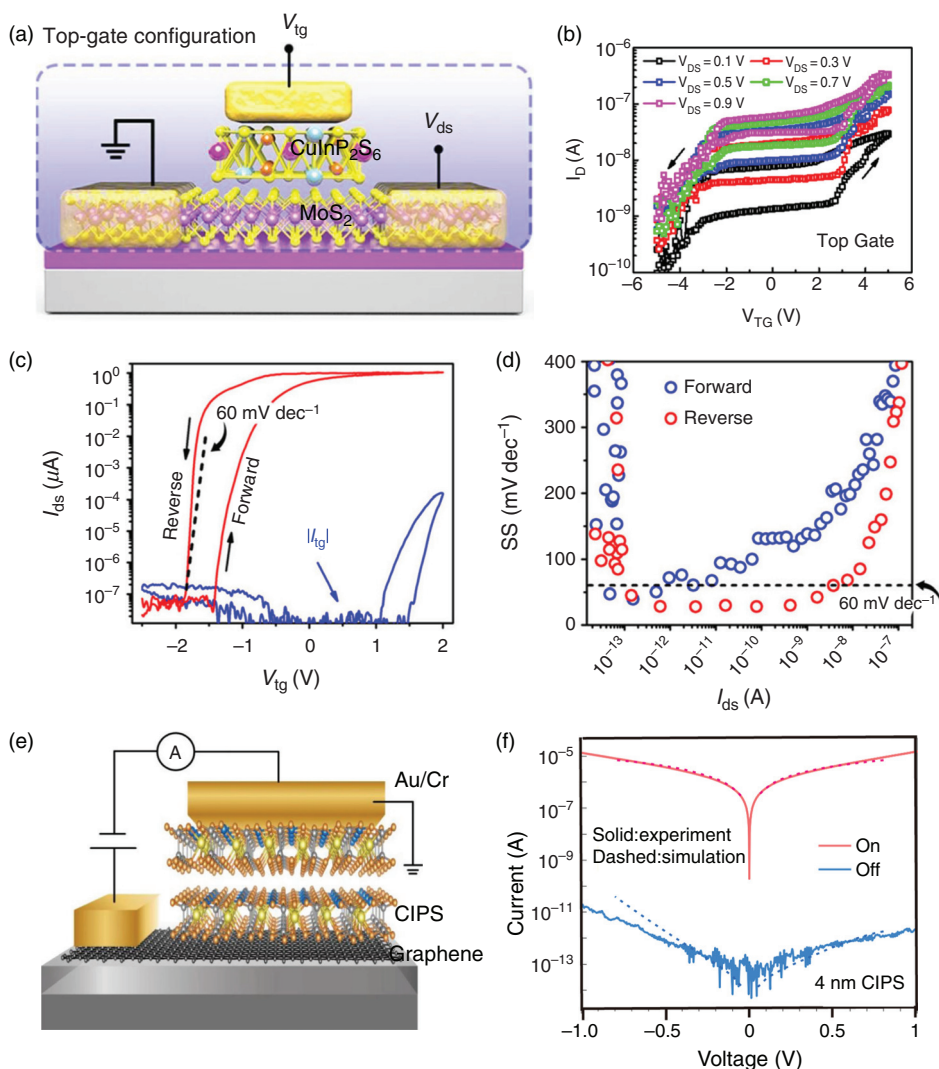


FIG. 12. VdW ferroelectric heterostructure based memory devices. (a) Schematic of vDW ferroelectric heterostructure based transistors where insulating vDW CuInP_2S_6 ferroelectric acts as a gate dielectric and MoS_2 serves as channel material. (b) I_D - V_{TG} transfer curves of a typical vDW ferroelectric heterostructure based transistor under different drain-source voltages. Reproduced with permission from Si *et al.*, ACS Nano **12**, 6700 (2018). Copyright 2018 American Chemical Society.⁵¹ (c) I_{ds} - V_{tg} transfer curves from another work and their corresponding leakage currents (blue). (d) Subthreshold swing with respect to I_{ds} . The data are extracted from (c). (a), (c), and (d) are reproduced with permission from Wang *et al.*, Nat. Commun. **10**, 3037 (2019). Copyright 2019 Springer Nature.¹⁰⁴ (e) Schematic of a ferroelectric tunnel junction made from vDW ferroelectric CuInP_2S_6 and graphene heterostructure. (f) Read tunneling current for on state and off state. (e) and (f) are reproduced with permission from Wu *et al.*, Nat. Electron. **3**, 466 (2020). Copyright 2020 Springer Nature.¹⁰⁶

can be conducted on (1) the enhancements of piezoelectric outputs for α - In_2Se_3 nanogenerators by, for instance, doping piezoelectric α - In_2Se_3 ; (2) piezotronic or piezophototronic device applications (the piezotronics refer to the strain-modulated carrier transport by the change in Schottky barrier height; the piezophotronics tune the generation, separation, and recommendation of photo-carriers by the strain-controlled Schottky barrier height).

IV. SUMMARY AND OUTLOOK

In terms of polarization origin, polar stabilization, and switching kinetics, the vDW ferroelectrics exhibit unprecedented physics compared to oxide ferroelectrics. These physical properties, which essentially stem from the vDW stacking and the weak interlayer interaction, suggest effective strategies to combat the notorious depolarization field. For instance, the interlayer-charge-transfer gives rise to the spontaneous polarization in 1T' WTe₂ rather than normal structural distortion and the screening of the depolarization field by interior free carriers, which allows switchable polarization to survive down to the

bilayer thickness. The dipole locking harnesses the exotic covalent bond configuration to resist the depolarization field and stabilizes the polarization switching in α - In_2Se_3 to a thickness as thin as the monolayer limit. The quadruple-well potential differs from the common double-well potential by possessing two additional wells related to Cu stable positions within CuInP_2S_6 vDW gaps. Its corresponding Cu ion migration likely accumulates charges at the interface, which contribute to the screening of the depolarization field and favors the stabilization of 4-nm ferroelectric switching in CuInP_2S_6 .

Other incorporated physical and chemical properties also broaden the scope of vDW ferroelectric physics by adding new ingredients into polarization switching. Piezoelectric domain walls, a new domain concept, arise from the natural existence of ferroelectric and antiferroelectric phases, which feature stronger piezoresponses at the boundaries but weaker piezoresponses within domains. The gate-tunable polarization enables the manipulation of ferroelectricity or ferroelectric domain walls through a gate bias, offering a new avenue to explore free-carrier-dependent polarization switching. Moreover, as

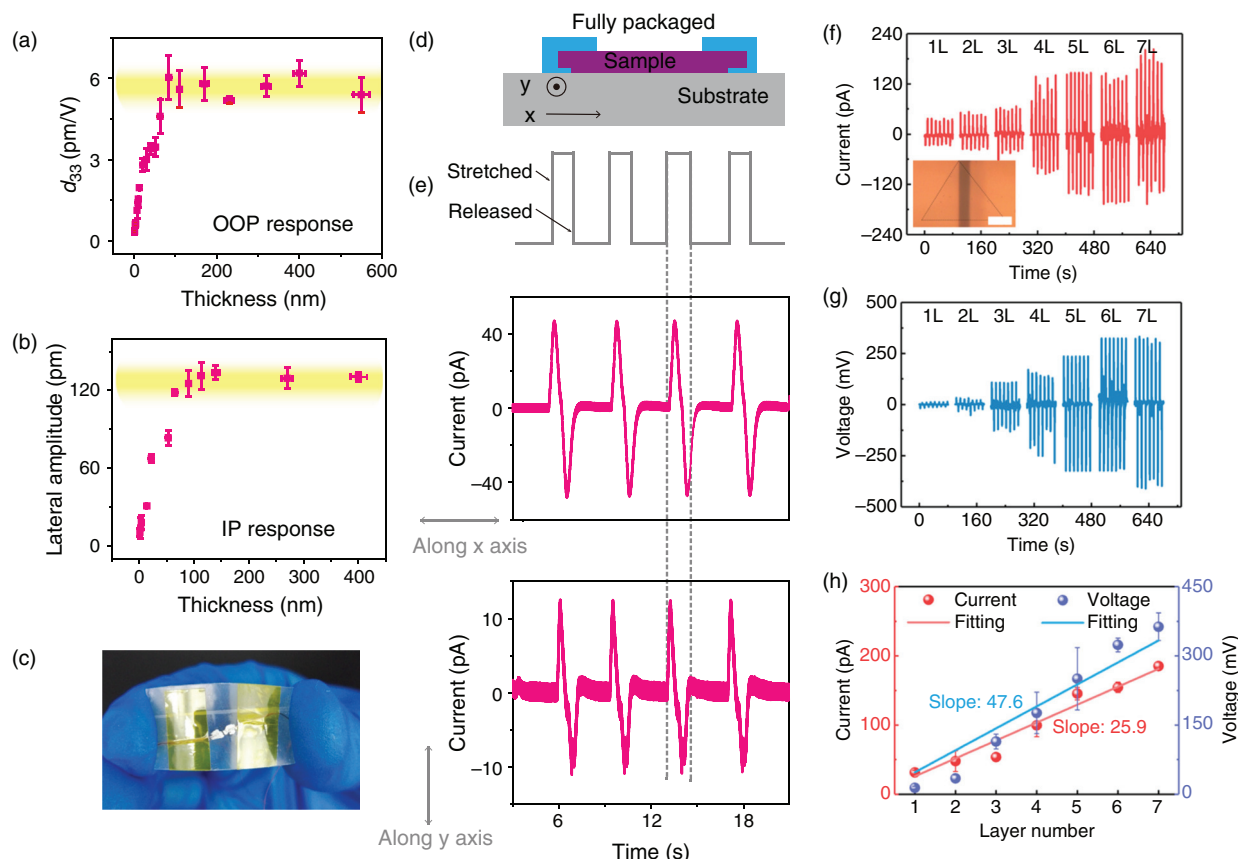


FIG. 13. Flexibly designed piezoelectric nanogenerators. Hexagonal α -In₂Se₃-based energy-harvesting device (a)–(e). (a) OOP piezoelectric constant and (b) IP piezoelectric response as a function of α -In₂Se₃ thickness. (c) Photo and (d) Schematic cross-section of the piezoelectric energy cell. (e) Electrical outputs for the device in (c). Reproduced with permission from Xue *et al.*, ACS Nano **12**, 4976 (2018). Copyright 2018 American Chemical Society.⁸⁴ Rhombohedral α -In₂Se₃-based energy-harvesting device (f)–(h). (f) Output currents and (g) output voltages as a function of sample thicknesses. (h) Peak currents and peak voltages with respect to sample thicknesses. Reproduced with permission from Dai *et al.*, Nano Lett. **19**, 5410 (2019). Copyright 2019 American Chemical Society.¹⁰⁷

vdW materials, layered ferroelectrics have no dangling bonds across the surfaces which provides an opportunity to flexibly construct ideal interfaces with two or more assembled different materials for more complicated electronic systems. Further, the vdW ferroelectrics are anticipated to extend Moore’s law for future electronics and optoelectronics,¹⁰⁸ and have shown promising applications in multifunctional memory devices, transistors, and energy-harvesting cells. Hence, the vdW ferroelectrics entail a new paradigm for both fundamental and technological exploration. However, much work remains to be done on this topic, which, in light of the material group, can be summarized as follows. We note that the outlook for the mentioned typical ferroelectrics can be extended to their corresponding family members.

In addition to ferroelectricity, the nonlinear anomalous Hall effect, Weyl semimetallicity, superconductivity, and non-saturating magnetoresistance are also found in the 1T’ WTe₂ crystal.^{66,69} Such fusion and subtlety motivate us to consider the following fundamental questions. Is there an intrinsic connection between ferroelectricity and these basic physical properties? If this connection exists, could ferroelectric switching be used to modulate them and spur memory device innovation? The answers to these questions need support and

validation through both theoretical and experimental methods. Additionally, the predicted ubiquitous effect, i.e., the interlayer charge transfer, also requires more experimental efforts made in non-polar 2D materials, such as h-BN. This effect will largely expand the ferroelectric material library beyond the prerequisites of non-centrosymmetry to paraelectric counterparts. Furthermore, even though the interlayer charge transfer has been unambiguously identified as the origin of 1T’ WTe₂ crystal, its switching dynamic still lacks an in-depth understanding. For example, how does a vertical poling electric field shift the IP interlayer sliding for polarization switching? How do the free movable electrons within 1T’ WTe₂ body influence switching? In addition, despite being in the same material family, the 1T’ WTe₂ and MoTe₂ exhibit different polarization origins (the latter origin is structural distortion) due to different atomic arrangements, which can be revealed from the fact that the polarization in monolayer WTe₂ vanishes while that in monolayer MoTe₂ surprisingly exists. In the transition metal dichalcogenide family, the investigation of ferroelectric switching in other semimetals, such as MoS₂, MoSe₂, and WS₂, will also be interesting. Finally, albeit the presence of ferroelectric switching in bilayer 1T’ WTe₂, the measurement was indeed

performed at a low temperature. Considering practical use, the room-temperature realization of bilayer ferroelectric switching is also a promising direction for future research. Regarding device application, since the 1T' WTe₂ is a metal, it is best to use its multilayer as “ferroelectric” electrodes for integrating with other functional 2D materials. For example, the 1T' WTe₂ and graphene can act as two separate electrodes to bridge MoS₂ for constructing ferroelectric-field-modulated photodetectors or solar cells. This design may be beneficial from the asymmetric Schottky barrier modulated by ferroelectric switching, vdW-contacted electrodes without damaging bonds across interfaces, which may lead the 1T' WTe₂ to develop high-performance ferroelectric heterostructure devices.

As the α -In₂Se₃ crystal is a displacive ferroelectric, the atomic visualization of its polar evolution under applied electric fields is highly desired, which can help further understand the dipole locking effect. The magnitude of ferroelectric polarization for both 3R and 2H α -In₂Se₃, and their associated thickness dependence also remain quantitatively unmeasured. Along these lines, the thickness-dependent IP polarization in 2H α -In₂Se₃ is under debate: through non-centrosymmetric analysis, one can observe that the IP polar of 2H phase may be canceled out in even layers while as evidenced from PFM measurement and IV curves, polarization exists in multilayers including even layers. Moreover, the systematic studies on the switching dynamics of α -In₂Se₃ ferroelectric polarization are intriguing and worthy of specific exploration; the manipulation of ferroelectric domain walls by gate biases and the in-depth investigation of the carriers’ effect on domain walls have not yet been done. Furthermore, future research on In₂Se₃ ferroelectric device applications could include the developments of high-quality material synthesis, high-performance device optimization, and high-density device array. We note that, since In₂Se₃ crystal has several polymorphisms, such as α , β , and γ , mixed-phase In₂Se₃ is usually synthesized using chemical methods when pure α -phase is intentionally grown. The controllable synthesis of single-phase, large-area α -In₂Se₃ is thus challenging but promising for scalable 2D memory fabrication. When large-size α -In₂Se₃ crystals are desired, an appealing application is to fabricate a crossbar-structured memristor array with multiple terminals for adaptive neuromorphic computing. Considering the excellent optical properties of α -In₂Se₃, such array devices are also anticipated to demonstrate neuromorphic vision systems and photonic in-memory computing chips integrating light sensing, logic, and memory. However, the single device performances of these device arrays such as switching time, retention, and endurance also need to be largely improved to at least approach commercial requirements. Regarding energy-harvesting applications, the piezoelectric outputs of α -In₂Se₃ nanogenerators should be thoroughly enhanced for example series circuits or material doping.

The movement of Cu ions in ferroelectric CuInP₂S₆ gives rise to some new puzzling questions as below. What are the behaviors of Cu ions in the vicinity of material interface? Is there charge accumulation at the interface as the charged Cu ion approaches the interface? Does the monolayer preserve switchable polarization? At the atomic monolayer, the switching behaviors may in part differ from those in the multilayer because the lack of vdW gaps likely restricts the Cu migration at the intralayer and produces new quantum phenomena. Aiming to resolve these unclear questions is indispensable for future progress. In addition, during ferroelectric switching, the influence of Cu

migration on tunnel transport across CuInP₂S₆ insulator is unexplored. The experimental demonstration of precise control of the four potential wells is an interesting direction that may be favorable for enhancing the density of ferroelectric information storage. The impact of sulfur vacancies on mobile Cu ions and potential curves remains elusive as well. With respect to the device applications, accessing the +HP and -HP of CuInP₂S₆ in a device architecture will be valuable for practical use. On the one hand, electrical access may boost the bias amplification effects of negative capacitance and lead to low-power transistors with steep subthreshold slopes. On the other hand, it can also enhance the electroresistance of ferroelectric tunnel junctions via the large ferroelectric modulation at the interface. Moreover, the access of +HP and -HP will also facilitate the realization of high piezoelectric outputs in flexible CuInP₂S₆ piezoelectric nanogenerators.

The task of examining a large number of predicted vdW ferroelectrics^{62,63,109} to find large polarization material also seems urgent because their experimental confirmed counterparts are not only scarce but also feature small polarization. Exploring vdW multiferroics is equally promising.^{39,79,110,111} Apart from intrinsic vdW multiferroicity, strategies based on theoretical calculation have been proposed for achieving non-intrinsic multiferroicity in vdW materials, for instance, artificially stacking vdW ferroelectrics and vdW ferrimagnetic, or doping vdW ferroelectrics with magnetic atoms. The experimental realization of either intrinsic or non-intrinsic vdW multiferroics would unlock the potential of next-generation computation.

ACKNOWLEDGMENTS

This work is supported by the King Abdullah University of Science and Technology with funding from Grant Nos. ORS-2016-CRG5-2996 and ORS-2018-CRG7-3717.

DATA AVAILABILITY

Data sharing is not applicable to this article as no new data were created or analyzed in this study.

REFERENCES

- ¹V. Garcia, S. Fusil, K. Bouzehouane, S. Enouz-Vedrenne, N. D. Mathur, A. Barthelemy, and M. Bibes, *Nature* **460**(7251), 81–84 (2009).
- ²H. Lu, C. W. Bark, D. E. de los Ojos, J. Alcalá, C. B. Eom, G. Catalan, and A. Gruber, *Science* **336**(6077), 59–61 (2012).
- ³Y. D. Liou, Y. Y. Chiu, R. T. Hart, C. Y. Kuo, Y. L. Huang, Y. C. Wu, R. V. Chopdekar, H. J. Liu, A. Tanaka, C. T. Chen, C. F. Chang, L. H. Tjeng, Y. Cao, V. Nagarajan, Y. H. Chu, Y. C. Chen, and J. C. Yang, *Nat. Mater.* **18**(6), 580–587 (2019).
- ⁴L. W. Martin and A. M. Rappe, *Nat. Rev. Mater.* **2**, 16087 (2016).
- ⁵N. Setter, D. Damjanovic, L. Eng, G. Fox, S. Gevorgian, S. Hong, A. Kingon, H. Kohlstedt, N. Y. Park, G. B. Stephenson, I. Stolitchnov, A. K. Taganstev, D. V. Taylor, T. Yamada, and S. Streiffer, *J. Appl. Phys.* **100**(5), 051606 (2006).
- ⁶W. Ji, K. Yao, and Y. C. Liang, *Adv. Mater.* **22**(15), 1763 (2010).
- ⁷J. E. Spanier, V. M. Fridkin, A. M. Rappe, A. R. Akbashev, A. Polemi, Y. B. Qi, Z. Q. Gu, S. M. Young, C. J. Hawley, D. Imbrenda, G. Xiao, A. L. Bennett-Jackson, and C. L. Johnson, *Nat. Photonics* **10**(9), 611–616 (2016).
- ⁸A. Chanthbouala, A. Crassous, V. Garcia, K. Bouzehouane, S. Fusil, X. Moya, J. Allibe, B. Dlubak, J. Grollier, S. Xavier, C. Deranlot, A. Moshar, R. Proksch, N. D. Mathur, M. Bibes, and A. Barthelemy, *Nat. Nanotechnol.* **7**(2), 101–104 (2011).
- ⁹W. J. Hu, Z. H. Wang, W. L. Yu, and T. Wu, *Nat Commun.* **7**, 10808 (2016).
- ¹⁰Y. L. Tang, Y. L. Zhu, X. L. Ma, A. Y. Borisevich, A. N. Morozovska, E. A. Eliseev, W. Y. Wang, Y. J. Wang, Y. B. Xu, Z. D. Zhang, and S. J. Pennycook, *Science* **348**(6234), 547–551 (2015).

- ¹¹C. T. Nelson, P. Gao, J. R. Jokisaari, C. Heikes, C. Adamo, A. Melville, S. H. Baek, C. M. Folkman, B. Winchester, Y. J. Gu, Y. M. Liu, K. Zhang, E. G. Wang, J. Y. Li, L. Q. Chen, C. B. Eom, D. G. Schlom, and X. Q. Pan, *Science* **334**(6058), 968–971 (2011).
- ¹²X. K. Wei, C. L. Jia, T. Sluka, B. X. Wang, Z. G. Ye, and N. Setter, *Nat. Commun.* **7**, 12385 (2016).
- ¹³H. Wang, Z. R. Liu, H. Y. Yoong, T. R. Paudel, J. X. Xiao, R. Guo, W. N. Lin, P. Yang, J. Wang, G. M. Chow, T. Venkatesan, E. Y. Tsymbal, H. Tian, and J. S. Chen, *Nat. Commun.* **9**, 3319 (2018).
- ¹⁴P. Gao, J. Britson, C. T. Nelson, J. R. Jokisaari, C. Duan, M. Trassin, S. H. Baek, H. Guo, L. Z. Li, Y. R. Wang, Y. H. Chu, A. M. Minor, C. B. Eom, R. Ramesh, L. Q. Chen, and X. Q. Pan, *Nat. Commun.* **5**, 3801 (2014).
- ¹⁵N. A. Hill, *J. Phys. Chem. B* **104**(29), 6694–6709 (2000).
- ¹⁶B. B. Van Aken, T. T. Palstra, A. Filippetti, and N. A. Spaldin, *Nat. Mater.* **3**(3), 164–170 (2004).
- ¹⁷J. Iniguez, P. Zubko, I. Luk'yanchuk, and A. Cano, *Nat. Rev. Mater.* **4**(4), 243–256 (2019).
- ¹⁸P. Marton, I. Rychetsky, and J. Hlinka, *Phys. Rev. B* **81**(14), 144125 (2010).
- ¹⁹D. Zhao, T. Lenz, G. H. Gelinck, P. Groen, D. Damjanovic, D. M. de Leeuw, and I. Katsouras, *Nat. Commun.* **10**, 2547 (2019).
- ²⁰K. J. Choi, M. Biegalski, Y. L. Li, A. Sharan, J. Schubert, R. Uecker, P. Reiche, Y. B. Chen, X. Q. Pan, V. Gopalan, L. Q. Chen, D. G. Schlom, and C. B. Eom, *Science* **306**(5698), 10005–10009 (2004).
- ²¹Y. J. Zhang, G. P. Li, T. Shimada, J. Wang, and T. Kitamura, *Phys. Rev. B* **90**(18), 184107 (2014).
- ²²N. Sai, A. M. Kolpak, and A. M. Rappe, *Phys. Rev. B* **72**(2), 020101(R) (2005).
- ²³A. Simon, J. Ravez, V. Maisonneuve, C. Payen, and V. B. Cajipe, *Chem. Mater.* **6**(9), 1575–1580 (1994).
- ²⁴F. C. Liu, L. You, K. L. Seyler, X. B. Li, P. Yu, J. H. Lin, X. W. Wang, J. D. Zhou, H. Wang, H. Y. He, S. T. Pantelides, W. Zhou, P. Sharma, X. D. Xu, P. M. Ajayan, J. L. Wang, and Z. Liu, *Nat. Commun.* **7**, 12357 (2016).
- ²⁵A. Belianinov, Q. He, A. Dziaugys, P. Maksymovych, E. Eliseev, A. Borisevich, A. Morozovska, J. Banys, Y. Vysochanskii, and S. V. Kalinin, *Nano Lett.* **15**(6), 3808–3814 (2015).
- ²⁶W. Ding, J. Zhu, Z. Wang, Y. Gao, D. Xiao, Y. Gu, Z. Zhang, and W. Zhu, *Nat. Commun.* **8**, 14956 (2017).
- ²⁷R. Fei, W. Kang, and L. Yang, *Phys. Rev. Lett.* **117**(9), 097601 (2016).
- ²⁸S. N. Shirodkar and U. V. Waghmare, *Phys. Rev. Lett.* **112**(15), 157601 (2014).
- ²⁹M. Wu and X. C. Zeng, *Nano Lett.* **17**(10), 6309–6314 (2017).
- ³⁰L. Li and M. Wu, *ACS Nano* **11**(6), 6382–6388 (2017).
- ³¹Y. Zhou, D. Wu, Y. Zhu, Y. Cho, Q. He, X. Yang, K. Herrera, Z. Chu, Y. Han, M. C. Downer, H. Peng, and K. Lai, *Nano Lett.* **17**(9), 5508–5513 (2017).
- ³²J. Xiao, H. Zhu, Y. Wang, W. Feng, Y. Hu, A. Dasgupta, Y. Han, Y. Wang, D. A. Muller, L. W. Martin, P. Hu, and X. Zhang, *Phys. Rev. Lett.* **120**(22), 227601 (2018).
- ³³C. Cui, W. J. Hu, X. Yan, C. Addiego, W. Gao, Y. Wang, Z. Wang, L. Li, Y. Cheng, P. Li, X. Zhang, H. N. Alshareef, T. Wu, W. Zhu, X. Pan, and L. J. Li, *Nano Lett.* **18**(2), 1253–1258 (2018).
- ³⁴S. Wan, Y. Li, W. Li, X. Mao, W. Zhu, and H. Zeng, *Nanoscale* **10**(31), 14885–14892 (2018).
- ³⁵F. Xue, W. Hu, K.-C. Lee, L.-S. Lu, J. Zhang, H.-L. Tang, A. Han, W.-T. Hsu, S. Tu, W.-H. Chang, C.-H. Lien, J.-H. He, Z. Zhang, L.-J. Li, and X. Zhang, *Adv. Funct. Mater.* **28**, 1803738 (2018).
- ³⁶Z. Fei, W. Zhao, T. A. Palomaki, B. Sun, M. K. Miller, Z. Zhao, J. Yan, X. Xu, and D. H. Cobden, *Nature* **560**(7718), 336–339 (2018).
- ³⁷X. Jiang, Y. Feng, K. Q. Chen, and L. M. Tang, *J. Phys. Condens. Matter* **32**(10), 105501 (2020).
- ³⁸S. M. Neumayer, E. A. Eliseev, M. A. Susner, A. Tselev, B. J. Rodriguez, J. A. Brehm, S. T. Pantelides, G. Panchapakesan, S. Jesse, S. V. Kalinin, M. A. McGuire, A. N. Morozovska, P. Maksymovych, and N. Balke, *Phys. Rev. Mater.* **3**(2), 024401 (2019).
- ³⁹J. Qi, H. Wang, X. Chen, and X. Qian, *Appl. Phys. Lett.* **113**(4), 043102 (2018).
- ⁴⁰J. R. Reimers, S. A. Tawfik, and M. J. Ford, *Chem. Sci.* **9**(39), 7620–7627 (2018).
- ⁴¹J. R. Rodriguez, W. Murray, K. Fujisawa, S. H. Lee, A. L. Kotrick, Y. Chen, N. McKee, S. Lee, M. Terrones, S. Trolier-McKinstry, T. N. Jackson, Z. Mao, Z. Liu, and Y. Liu, *Appl. Phys. Lett.* **117**(5), 052901 (2020).
- ⁴²W. F. Io, S. Yuan, S. Y. Pang, L. W. Wong, J. Zhao, and J. Hao, *Nano Res.* **13**(7), 1897–1902 (2020).
- ⁴³Y. Bao, P. Song, Y. P. Liu, Z. H. Chen, M. L. Zhu, I. Abdelwahab, J. Su, W. Fu, X. Chi, W. Yu, W. Liu, X. X. Zhao, Q. H. Xu, M. Yang, and K. P. Loh, *Nano Lett.* **19**(8), 5109–5117 (2019).
- ⁴⁴H. Yang, M. Q. Xiao, Y. Cui, L. F. Pan, K. Zhao, and Z. M. Wei, *Sci. China Inf. Sci.* **62**(12), 220404 (2019).
- ⁴⁵R. Rashid, F. C. Ling, S. P. Wang, K. Xiao, X. Cui, T. H. Chan, H. C. Ong, W. Azeem, and M. Younas, *Nanoscale* **12**, 20189 (2020).
- ⁴⁶K. C. Kwon, Y. S. Zhang, L. Wang, W. Yu, X. J. Wang, I. H. Park, H. S. Choi, T. Ma, Z. Y. Zhu, B. B. Tian, C. L. Su, and K. P. Loh, *ACS Nano* **14**(6), 7628–7638 (2020).
- ⁴⁷M. W. Si, A. K. Saha, S. J. Gao, G. Qiu, J. K. Qin, Y. Q. Duan, J. Jian, C. Niu, H. Y. Wang, W. Z. Wu, S. K. Gupta, and P. D. D. Ye, *Nat. Electron.* **2**(12), 580–586 (2019).
- ⁴⁸N. Higashitaramizu, H. Kawamoto, C. J. Lee, B. H. Lin, F. H. Chu, I. Yonemori, T. Nishimura, K. Wakabayashi, W. H. Chang, and K. Nagashio, *Nat. Commun.* **11**(1), 2428 (2020).
- ⁴⁹S. Guan, C. Liu, Y. H. Lu, Y. G. Yao, and S. A. Yang, *Phys. Rev. B* **97**(14), 144104 (2018).
- ⁵⁰M. Si, A. K. Saha, P. Y. Liao, S. Gao, S. M. Neumayer, J. Jian, J. Qin, N. Balke Wisinger, H. Wang, P. Maksymovych, W. Wu, S. K. Gupta, and P. D. Ye, *ACS Nano* **13**(8), 8760–8765 (2019).
- ⁵¹M. W. Si, P. Y. Liao, G. Qiu, Y. Q. Duan, and P. D. D. Ye, *ACS Nano* **12**(7), 6700–6705 (2018).
- ⁵²L. You, F. Liu, H. Li, Y. Hu, S. Zhou, L. Chang, Y. Zhou, Q. Fu, G. Yuan, S. Dong, H. J. Fan, A. Gruverman, Z. Liu, and J. Wang, *Adv. Mater.* **30**(51), e1803249 (2018).
- ⁵³Y. Wang, C. C. Xiao, M. G. Chen, C. Q. Hu, J. D. Zou, C. Wu, J. Z. Jiang, S. Y. A. Yang, Y. H. Lu, and W. Ji, *Mater. Horizons* **5**(3), 521–528 (2018).
- ⁵⁴K. Chang, F. Kuster, B. J. Miller, J. R. Ji, J. L. Zhang, P. Sessi, S. Barraza-Lopez, and S. S. P. Parkin, *Nano Lett.* **20**(9), 6590–6597 (2020).
- ⁵⁵C. Xu, Y. Chen, X. Cai, A. Meingast, X. Guo, F. Wang, Z. Lin, T. W. Lo, C. Maunders, S. Lazar, N. Wang, D. Lei, Y. Chai, T. Zhai, X. Luo, and Y. Zhu, *Phys. Rev. Lett.* **125**(4), 047601 (2020).
- ⁵⁶A. Dziaugys, K. Kelley, J. A. Brehm, L. Tao, A. Puretzky, T. Feng, A. O'Hara, S. Neumayer, M. Chyasnavichyus, E. A. Eliseev, J. Banys, Y. Vysochanskii, F. Ye, B. C. Chakoumakos, M. A. Susner, M. A. McGuire, S. V. Kalinin, P. Ganesh, N. Balke, S. T. Pantelides, A. N. Morozovska, and P. Maksymovych, *Nat. Commun.* **11**(1), 3623 (2020).
- ⁵⁷F. Xue, X. He, J. R. D. Retamal, A. L. Han, J. W. Zhang, Z. X. Liu, J. K. Huang, W. J. Hu, V. Tung, R. H. He, L. J. Li, and X. X. Zhang, *Adv. Mater.* **31**(29), 1901300 (2019).
- ⁵⁸F. Xue, X. He, W. H. Liu, D. Periyangounder, C. H. Zhang, M. G. Chen, C. H. Lin, L. Q. Luo, E. Yengel, V. Tung, T. D. Anthopoulos, L. J. Li, J. H. He, and X. X. Zhang, *Adv. Funct. Mater.* **30**(20), 2004206 (2020).
- ⁵⁹C. Paillard, X. F. Bai, I. C. Infante, M. Guennou, G. Geneste, M. Alexe, J. Kreisel, and B. Dkhil, *Adv. Mater.* **28**(26), 5153–5168 (2016).
- ⁶⁰C. J. Cui, F. Xue, W. J. Hu, and L. J. Li, *NPJ 2D Mater. Appl.* **2**, 1–14 (2018).
- ⁶¹Z. Guan, H. Hu, X. W. Shen, P. H. Xiang, N. Zhong, J. H. Chu, and C. G. Duan, *Adv. Electron. Mater.* **6**(1), 1900818 (2020).
- ⁶²J. Shang, X. Tang, and L. Kou, *WIRES Comput. Mol. Sci.* **11**(2), e1496 (2020).
- ⁶³M. Wu and P. Jena, *WIRES Comput. Mol. Sci.* **8**(5), e1365 (2018).
- ⁶⁴Z. Ni, E. Minamitani, K. Kawahara, R. Arafune, C.-L. Lin, N. Takagi, and S. Watanabe, *J. Phys. Chem. C* **124**(3), 2008–2012 (2019).
- ⁶⁵Q. Yang, M. H. Wu, and J. Li, *J. Phys. Chem. Lett.* **9**(24), 7160–7164 (2018).
- ⁶⁶W. X. Zhou and A. Ariando, *Japanese J. Appl. Phys.* **59**(SI), SI0802 (2020).
- ⁶⁷Y. Wang, X. H. Liu, J. D. Burton, S. S. Jaswal, and E. Y. Tsymbal, *Phys. Rev. Lett.* **109**(24), 247601 (2012).
- ⁶⁸P. Sharma, F. X. Xiang, D. F. Shao, D. W. Zhang, E. Y. Tsymbal, A. R. Hamilton, and J. Seidel, *Sci. Adv.* **5**(7), eaax5080 (2019).
- ⁶⁹H. Wang and X. Qian, *NPJ Comput. Mater.* **5**(1), 119 (2019).
- ⁷⁰I. Pletikosic, M. N. Ali, A. V. Fedorov, R. J. Cava, and T. Valla, *Phys. Rev. Lett.* **113**(21), 216601 (2014).
- ⁷¹P. Li, Y. Wen, X. He, Q. Zhang, C. Xia, Z. M. Yu, S. Y. A. Yang, Z. Y. Zhu, H. N. Alshareef, and X. X. Zhang, *Nat. Commun.* **8**, 2150 (2017).

- ⁷²S. J. Tang, C. F. Zhang, D. Wong, Z. Pedramrazi, H. Z. Tsai, C. J. Jia, B. Moritz, M. Claassen, H. Ryu, S. Kahn, J. Jiang, H. Yan, M. Hashimoto, D. H. Lu, R. G. Moore, C. C. Hwang, C. Hwang, Z. Hussain, Y. L. Chen, M. M. Ugeda, Z. Liu, X. M. Xie, T. P. Devereaux, M. F. Crommie, S. K. Mo, and Z. X. Shen, *Nat. Phys.* **13**(7), 683+ (2017).
- ⁷³Z. R. Zheng, Q. Ma, Z. Bi, S. de la Barrera, M. H. Liu, N. N. Mao, Y. Zhang, N. Kiper, K. Watanabe, T. Taniguchi, J. Kong, W. A. Tisdale, R. Ashoori, N. Gedik, L. Fu, S. Y. Xu, and P. Jarillo-Herrero, *Nature* **588**(7836), 71+ (2020).
- ⁷⁴S. Yuan, X. Luo, H. L. Chan, C. Xiao, Y. Dai, M. Xie, and J. Hao, *Nat. Commun.* **10**(1), 1775 (2019).
- ⁷⁵T. R. Chang, S. Y. Xu, G. Chang, C. C. Lee, S. M. Huang, B. Wang, G. Bian, H. Zheng, D. S. Sanchez, I. Belopolski, N. Alidoust, M. Neupane, A. Bansil, H. T. Jeng, H. Lin, and M. Z. Hasan, *Nat. Commun.* **7**, 10639 (2016).
- ⁷⁶Y. P. Qi, P. G. Naumov, M. N. Ali, C. R. Rajamathi, W. Schnelle, O. Barkalov, M. Hanfland, S. C. Wu, C. Shekhar, Y. Sun, V. Suss, M. Schmidt, U. Schwarz, E. Pippel, P. Werner, R. Hillebrand, T. Forster, E. Kampert, S. Parkin, R. J. Cava, C. Felser, B. H. Yan, and S. A. Medvedev, *Nat. Commun.* **7**, 11038 (2016).
- ⁷⁷J. Peng, Y. H. Liu, X. Luo, J. J. Wu, Y. Lin, Y. Q. Guo, J. Y. Zhao, X. J. Wu, C. Z. Wu, and Y. Xie, *Adv. Mater.* **31**(19), 1900568 (2019).
- ⁷⁸M. J. Dai, K. Li, F. K. Wang, Y. X. Hu, J. Zhang, T. Y. Zhai, B. Yang, Y. Q. Fu, W. W. Cao, D. C. Jia, Y. Zhou, and P. A. Hu, *Adv. Electron. Mater.* **6**(2), 1900975 (2020).
- ⁷⁹C. Gong, E. M. Kim, Y. Wang, G. Lee, and X. Zhang, *Nat. Commun.* **10**(1), 2657 (2019).
- ⁸⁰Y. Li, C. Chen, W. Li, X. Y. Mao, H. Liu, J. Y. Xiang, A. M. Nie, Z. Y. Liu, W. G. Zhu, and H. L. Zeng, *Adv. Electron. Mater.* **6**(7), 2000061 (2020).
- ⁸¹L. Liu, J. Dong, J. Huang, A. Nie, K. Zhai, J. Xiang, B. Wang, F. Wen, C. Mu, Z. Zhao, Y. Gong, Y. Tian, and Z. Liu, *Chem. Mater.* **31**(24), 10143–10149 (2019).
- ⁸²S. M. Poh, S. J. R. Tan, H. Wang, P. Song, I. H. Abidi, X. Zhao, J. D. Dan, J. S. Chen, Z. T. Luo, S. J. Pennycook, A. H. C. Neto, and K. P. Loh, *Nano Lett.* **18**(10), 6340–6346 (2018).
- ⁸³L. Wang, X. Wang, Y. Zhang, R. Li, T. Ma, K. Leng, Z. Chen, I. Abdelwahab, and K. P. Loh, *Adv. Funct. Mater.* **30**, 2004609 (2020).
- ⁸⁴F. Xue, J. Zhang, W. Hu, W. T. Hsu, A. Han, S. F. Leung, J. K. Huang, Y. Wan, S. Liu, J. Zhang, J. H. He, W. H. Chang, Z. L. Wang, X. Zhang, and L. J. Li, *ACS Nano* **12**(5), 4976–4983 (2018).
- ⁸⁵Y. Li, M. Gong, and H. Zeng, *J. Semicond.* **40**(6), 061002 (2019).
- ⁸⁶S. Y. Wan, Y. Li, W. Li, X. Y. Mao, C. Wang, C. Chen, J. Y. Dong, A. M. Nie, J. Y. Xiang, Z. Y. Liu, W. G. Zhu, and H. L. Zeng, *Adv. Funct. Mater.* **29**(20), 1808606 (2019).
- ⁸⁷K. Xu, W. Jiang, X. S. Gao, Z. J. Zhao, T. Low, and W. J. Zhu, *Nanoscale* **12**(46), 23488–23496 (2020).
- ⁸⁸S. Raj Panday and B. M. Fregoso, *J. Phys. Condens. Matter* **29**(43), 43LT01 (2017).
- ⁸⁹B. Lv, Z. Yan, W. Xue, R. Yang, J. Li, W. Ci, R. Pang, G. Liu, P. Zhou, Z. Liu, W. Zhu, and X. Xu, “Layer-dependent ferroelectricity in 2H-stacked few-layer α -In₂Se₃,” *Mater. Horiz.* (published online) (2021).
- ⁹⁰M. Hoffmann, F. P. G. Fengler, M. Herzig, T. Mittmann, B. Max, U. Schroeder, R. Negrea, P. Lucian, S. Slesazeck, and T. Mikolajick, *Nature* **565**(7740), 464–467 (2019).
- ⁹¹J. A. Brehm, S. M. Neumayer, L. Tao, A. O’Hara, M. Chyasanavichus, M. A. Susner, M. A. McGuire, S. V. Kalinin, S. Jesse, P. Ganesh, S. T. Pantelides, P. Maksymovych, and N. Balke, *Nat. Mater.* **19**(1), 43–48 (2020).
- ⁹²N. Balke, S. M. Neumayer, J. A. Brehm, M. A. Susner, B. J. Rodriguez, S. Jesse, S. V. Kalinin, S. T. Pantelides, M. A. McGuire, and P. Maksymovych, *ACS Appl. Mater. Interfaces* **10**(32), 27188–27194 (2018).
- ⁹³L. You, Y. Zhang, S. Zhou, A. Chaturvedi, S. A. Morris, F. C. Liu, L. Chang, D. Ichinose, H. Funakubo, W. J. Hu, T. Wu, Z. Liu, S. Dong, and J. L. Wang, *Sci. Adv.* **5**(4), eaav3780 (2019).
- ⁹⁴J. Deng, Y. Liu, M. Li, S. Xu, Y. Lun, P. Lv, T. Xia, P. Gao, X. Wang, and J. Hong, *Small* **16**(1), e1904529 (2020).
- ⁹⁵W. Huang, F. Wang, L. Yin, R. Cheng, Z. Wang, M. G. Sendeku, J. Wang, N. Li, Y. Yao, and J. He, *Adv. Mater.* **32**(14), e1908040 (2020).
- ⁹⁶S. Zhou, L. You, A. Chaturvedi, S. A. Morris, J. S. Herrin, N. Zhang, A. Abdelsamie, Y. Hu, J. Chen, Y. Zhou, S. Dong, and J. Wang, *Mater. Horiz.* **7**(1), 263–274 (2020).
- ⁹⁷S. Zhou, L. You, H. Zhou, Y. Pu, Z. Gui, and J. Wang, *Front. Phys.* **16**(1), 13301 (2021).
- ⁹⁸S. M. Neumayer, L. Tao, A. O’Hara, J. Brehm, M. Si, P.-Y. Liao, T. Feng, S. V. Kalinin, P. D. Ye, S. T. Pantelides, P. Maksymovych, and N. Balke, *Phys. Rev. Appl.* **13**(6), 064063 (2020).
- ⁹⁹S. M. Neumayer, L. Tao, A. O’Hara, M. A. Susner, M. A. McGuire, P. Maksymovych, S. T. Pantelides, and N. Balke, *Adv. Energy Mater.* **10**(39), 2001726 (2020).
- ¹⁰⁰D. Lee, E. Hwang, Y. Lee, Y. Choi, J. S. Kim, S. Lee, and J. H. Cho, *Adv. Mater.* **28**(41), 9196–9202 (2016).
- ¹⁰¹J. Lee, S. Pak, Y. W. Lee, Y. Cho, J. Hong, P. Giraud, H. S. Shin, S. M. Morris, J. I. Sohn, S. Cha, and J. M. Kim, *Nat. Commun.* **8**, 14734 (2017).
- ¹⁰²K. Roy, M. Padmanabhan, S. Goswami, T. P. Sai, G. Ramalingam, S. Raghavan, and A. Ghosh, *Nat. Nanotechnol.* **8**(11), 826–830 (2013).
- ¹⁰³Y. T. Lee, H. Kwon, J. S. Kim, H. H. Kim, Y. J. Lee, J. A. Lim, Y. W. Song, Y. Yi, W. K. Choi, D. K. Hwang, and S. Im, *ACS Nano* **9**(10), 10394–10401 (2015).
- ¹⁰⁴X. Wang, P. Yu, Z. Lei, C. Zhu, X. Cao, F. Liu, L. You, Q. Zeng, Y. Deng, C. Zhu, J. Zhou, Q. Fu, J. Wang, Y. Huang, and Z. Liu, *Nat. Commun.* **10**(1), 3037 (2019).
- ¹⁰⁵H. Ryu, K. Xu, D. Li, X. Hong, and W. Zhu, *Appl. Phys. Lett.* **117**(8), 080503 (2020).
- ¹⁰⁶J. Wu, H.-Y. Chen, N. Yang, J. Cao, X. Yan, F. Liu, Q. Sun, X. Ling, J. Guo, and H. Wang, *Nat. Electron.* **3**(8), 466–472 (2020).
- ¹⁰⁷M. Dai, Z. Wang, F. Wang, Y. Qiu, J. Zhang, C. Y. Xu, T. Zhai, W. Cao, Y. Fu, D. Jia, Y. Zhou, and P. A. Hu, *Nano Lett.* **19**(8), 5410–5416 (2019).
- ¹⁰⁸M. Y. Li, S. K. Su, H. S. P. Wong, and L. J. Li, *Nature* **567**(7747), 169–170 (2019).
- ¹⁰⁹X.-Y. Ma, H.-Y. Lyu, K.-R. Hao, Y.-M. Zhao, X. Qian, Q.-B. Yan, and G. Su, *Sci. Bull.* **66**(3), 233–242 (2021).
- ¹¹⁰J.-M. Liu, M. Wu, X. Li, and T. Zhong, *Nat. Sci. Rev.* **7**(2), 373–380 (2020).
- ¹¹¹H. Yang, L. F. Pan, M. Q. Xiao, J. Z. Fang, Y. Cui, and Z. M. Wei, *Sci. China Mater.* **63**(3), 421–428 (2020).